Negative cell cycle regulation by Calcineurin is necessary for proper beta cell regeneration in zebrafish

Laura Massoz[1*], David Bergemann[1], Arnaud Lavergne[1,2], Célia Reynders[1], Caroline Désiront[1], Chiara Goossens[1], Lydie Flasse[1], Bernard Peers[1], Marianne L. Voz[1] and Isabelle Manfroid[1]

Author Affiliations

[1]Zebrafish Development and Disease Models laboratory, GIGA-Stem Cells, University of Liège, Liège, Belgium

[2]GIGA-Genomics core facility, GIGA, University of Liège, Liège, Belgium

*Corresponding author:

Email address: laura.massoz@doct.uliege.be

Abstract

Stimulation of pancreatic beta cell regeneration could be a therapeutic lead to treat diabetes. Unlike humans, the zebrafish can efficiently regenerate beta cells, notably from ductal pancreatic progenitors. To gain insight into the molecular pathways involved in this process, we established the transcriptomic profile of the ductal cells after beta cell ablation in the adult zebrafish. These data highlighted the protein phosphatase calcineurin as a new potential modulator of beta cell regeneration. We showed that calcineurin overexpression abolished the regenerative response, leading to glycemia dysregulation. On the opposite, calcineurin inhibition increased ductal cell proliferation and subsequent beta cell regeneration. Interestingly, the enhanced proliferation of the progenitors was paradoxically coupled with their exhaustion. This suggests that the proliferating progenitors are next entering in differentiation. Calcineurin appears as a guardian which prevents an excessive progenitor proliferation to preserve the pool of progenitors. Altogether, our findings reveal calcineurin as a key player in the balance between proliferation and differentiation to enable a proper beta cell regeneration.

Introduction

Blood glucose homeostasis is tightly controlled by pancreatic endocrine cells. Insulin-producing beta cells work in close association with alpha cells, which secrete glucagon, and delta cells secreting somatostatin, to maintain normal glycemia. The insulin plays a critical role in this process as it is the only hormone able to lower the glycemia. Beta cell loss is a hallmark of type 1 and of late stages of type 2 diabetes, leading to chronic hyperglycemia. Beta cell destruction is largely irreversible in human and in mammals, making the disease incurable nowadays. Nevertheless, studies in diabetic mice models uncovered promising evidences of slight recovery of beta cells via regeneration. For example, new beta cells can arise from the replication of remaining beta cells [1]. Different models of pancreas injuries revealed the plasticity of mammalian pancreatic cells. Actually, differentiated endocrine cells such as alpha cells[2] and delta cells[3] can reprogram and convert into insulin-producing cells, a process that is age dependent. Another possible source of beta cells could be de *novo* formation from pancreatic progenitors residing in the ductal compartment of the adult pancreas [4]. Lineage tracing experiments could not clearly highlight new beta cells arising from the ductal cells in the adult [4]–[6]. However, expression of the pro-endocrine marker Neurog3 was detected in the ducts in different mouse models of pancreas regeneration [4], [7], [8]. In addition, a rare population of ductal cells expressing Neurog3 has been reported to contribute to beta cell neogenesis during diabetes [9]. A recent study of single cell RNA sequencing reveal a sub-population of human ductal cells which are

able to give rise to all the pancreatic cell types, including beta cells, following implantation in mice [10]. Altogether, these findings suggest that mammalian pancreatic ducts possess the intrinsic capacity to (re)generate beta cells even though this process is poorly efficient and slow, especially in adults. In contrast to mammals, zebrafish possess remarkable capacity of regeneration, independently of its age [11]–[16]. This model can therefore be exploited to identify and characterize regenerative mechanisms and ultimately induce regeneration in mammals. Based on regenerative mechanisms identified in zebrafish, several studies succeed to improve regeneration in mammals, underlying the possibility of translation from zebrafish to mammals ([17]–[21] and [22], for review).

In zebrafish, the nitroreductase (NTR)/nitroaromatic prodrug system is widely used. In this technique, the combination of cell type-specific NTR expression and nitroaromatic prodrug exposure allow for controlled and targeted cell ablation [23], [24]. When NTR is expressed under the control of the *insulin* (*ins*) promoter (*Tg*(*ins:NTR-mCherry*) [25]), beta cell destruction is complete within 3 days following the treatment in adult fish, which correlate with a peak of hyperglycemia [26], [27]. The regeneration of beta cells upon ablation is spontaneous and fast and the glycemia is normalized within two weeks [13], [29]. Similar to mice, new beta cells can arise through proliferation of surviving beta cells [28] as well as through the contribution of alpha cells [29], [30] and delta cells[31], [32], underscoring the overall conservation of these processes from zebrafish to mammals. Nevertheless, unlike mammals, the presence of pancreatic progenitors in the ducts is well established in both larval [33] and adult zebrafish [26], [27]. Lineage tracing experiments pointed out that ductal cells and centroacinar cells (CACs) give rise to new beta cells [26], [33]. In adults, duct-derived beta cells start to be detected between 7 and 10 days following beta cell ablation [26], [27].

Notch signaling is a key player regulating the differentiation of duct-associated progenitors into endocrine cells. Larval duct cells as well as adult CACs display strong Notch activity [26], [34]. This signaling pathway has a central role in beta cell genesis during both development [35] and regeneration [33] by repressing endocrine differentiation. In zebrafish, different levels of Notch activity determine the behavior of the pancreatic progenitors. While a high level of Notch activity maintains cells in quiescence, a moderate level induces the entry in the cell cycle and proliferation whereas a low level drives endocrine differentiation of the progenitor cells [35]. A steep decrease of Notch activity pushes the progenitors to differentiate prematurely, bypassing the amplification step and leading to their depletion [35]. Repression of the Notch signaling by mTor, activated by glucose and nutrients, hence promotes beta cell formation and regeneration from ductal progenitors [33]. While Notch and mTor signaling are crucial for this process, there is still a need to establish a global view of the molecular mechanisms regulating beta cell regeneration.

93 To identify early events regulating ductal-derived beta cell regeneration, we determined the
94 transcriptomic signature of ductal cells from adult zebrafish following beta cell destruction. Our data
95 highlighted an upregulation of the Calcineurin (CaN) pathway. To elucidate CaN function in beta cell
96 regeneration, we both repressed and activated CaN pathway. We showed that CaN regulates beta cell
97 neogenesis in the ducts during regeneration, by acting on progenitor proliferation. Together, our
98 findings underline that CaN fine tunes the balance between progenitor proliferation and beta cell
99 differentiation to guarantee proper regeneration.

100

101 **Results**

102 *Transcriptomic profiling of ductal cells after beta cell destruction highlights regulation of calcineurin*
103 *pathway*

104 To gain a better understanding of the molecular mechanisms underlying the regeneration of beta cells
105 from the ducts, we determined the transcriptional landscape of ductal cells by RNA-sequencing after
106 beta cell ablation in the adult zebrafish. To selectively ablate the beta cells, we used the *Tg*(*ins:NTR-*
107 *mCherry*) transgenic fish. The ductal cells were labelled thanks to the *Tg*(*nkx6.1:GFP*) reporter line [27]
108 in which GFP marks the ductal tree and associated multipotent pancreatic progenitors [27]. More
109 precisely, 3 to 4 fishes were treated with the pro-drug MTZ at 10mM overnight, to induce ablation of
110 beta cells or with DMSO for the non-ablated controls. Ablation was confirmed by blood glucose
111 measurement before collection of the pancreas. To capture the early events triggered by the
112 destruction of beta cells, we generated the transcriptome of the ducts 3 days post ablation treatment
113 (dpt), *i.e.* before beta cell neogenesis (**Figure 1A supplemental**). Differential gene expression analysis
114 revealed that 1866 genes are up-regulated and 1515 genes down-regulated in the ductal cell of fish
115 treated with MTZ compared to control (pAdj < 0.05). According to Gene Ontology analysis, the most
116 enriched pathways among the up-regulated genes were DNA replication and cell cycle (**Figure 1A**). This
117 further corroborates our previous findings and those of others, regarding the activation of duct-
118 associated progenitors' proliferation in response to beta cell ablation [26], [27]. As expected, the Notch
119 pathway was enriched in the down-regulated genes [33], [35] (**Figure 1B**). On a contrasting note, in a
120 context marked by a robust proliferative response, we found it intriguing to observe an enrichment in
121 the cellular senescence signature (**Figure 1A**). Subsequently, we investigated deeper into the genes
122 associated with this specific signature. We found among them several components of the calcineurin
123 signaling pathway such as *nfatc3b*, *ppp3ccb* (the catalytic subunit of Calcineurin*), itpr2* and *calm3b*
124 **(Figure 1C)**. In addition to these genes related to the cellular senescence signature, our transcriptomic
125 studies revealed the modulation of other genes from the CaN canonical pathway (**Figure 1D**),
126 underlying its potential role in beta cell regeneration. Calcineurin (CaN) is a highly conserved

127 calcium/calmodulin dependent Ser/Thr phosphatase, involved in numerous biological process
128 including fin regeneration and beta cell function [36]–[39]. This prompted us to investigate the role of
129 CaN in beta cell regeneration.

130 Previous RNAseq data performed in our laboratory indicate that CaN (*ppp3cca/b*) and NFATc3
131 (*nfatc3a/b*) are mainly express in endocrine cells [40] (**Figure 1B supplemental**), which is in accordance
132 with the role of CaN/NFAT signalling in beta cells [41]. CaN genes (*ppp3cca/b*) as well as *nfatc3b,* are
133 express at lower levels in the ducts at basal state but their expression is induced in response to beta
134 cell destruction (**Figure 1C supplemental**).

135 *Calcineurin activity regulates the ductal regenerative response*

136 To evaluate the role of CaN in beta cell regeneration, more specifically derived from ductal progenitors,
137 we have chosen to use young larvae, where regenerated beta cells in the pancreatic tail arise
138 exclusively from the ducts [33]. In response to beta cells ablation, the intrapancreatic ducts undergo a
139 ductal regenerative response whereby differentiation toward the endocrine fate is increased [33]. We
140 first determined the rate of beta cell neogenesis from the ducts in response to a single acute ablation
141 of beta cells as we performed in adults. We treated *Tg*(*ins:NTR-P2A-mCherry*); *Tg*(*nkx6.1:GFP*) larvae
142 with nifurpirinol (NFP) from 3 to 4 dpf and mCherry+ beta cells were quantified in the GFP+ ducts in
143 the pancreatic tail at several time points: 4, 7, 10 and 14 dpt (**Figure 1E**). Duct-associated beta cells
144 started to be detected in non-ablated larvae between 7 and 10 dpt (**Figure 1F**) and the number of beta
145 cells slowly increased until 14 dpt (**Figure 1F, 1G**). In ablated larvae, the increase became more
146 pronounced from 10 dpt onwards (**Figure 1F, 1G**), indicating faster endocrine differentiation. This
147 experiment establishes that the ductal regenerative response is detectable between 10 and 14 days
148 after the beta cell ablation, performed at 3 dpf. We next wanted to determine if ductal cell proliferation
149 is activated in response to beta cell destruction in larvae as in adult fish. We exposed *Tg(ins:NTR-P2A-*
150 *mCherry); Tg(nkx6.1:GFP)* larvae to EdU the second day following ablation (**Figure 1H**). In the ablated
151 larvae, the proportion of GFP+ ductal cells EdU+ (in S-phase) was higher compared to non-ablated
152 larvae (**Figure 1I, 1J**). This result shows that acute beta cell ablation in larvae rapidly activates ductal
153 cell proliferation, as previously reported in adult zebrafish.

154 As our transcriptomic data from adult zebrafish revealed modulation of the CaN pathway at 3 dpt
155 (**Figure 1D**), we treated *Tg*(*ins:NTR-P2A-mCherry*); *Tg*(*nkx6.1:GFP*) larvae from 1 to 3 dpt after beta cell
156 ablation, with a CaN inhibitor, the Cyclosporin A (CsA) [39] (**Figure 2A**). The number of newly formed
157 beta cells in the tail was monitored from 4 to 14 dpt. CsA enhanced beta cell formation at 10 dpt (**Figure**
158 **2B-D)**. However, this effect appears to be transient since no discernible difference was observed
159 between the control and CsA-treated larvae in regeneration at the latest time point (14dpt), suggesting

160 an acceleration of the regenerative response (**Figure 2B, Figure 2A supplemental**). Interestingly, CsA
161 did not affect beta cell differentiation in non-ablated larvae, indicating that CsA only acts in a
162 regenerative context (**Figure 2B-D)**. Of note, CsA increased as well the number of regenerated beta
163 cells in the principal islet (**Figure 2B, 2C supplemental**). We and others, previously showed that the
164 other major source of beta cell regeneration, besides the ducts, are the bi-hormonal sst1.1+/ins+ cells
165 [31], [32], [42]. However, CsA did not affect bi-hormonal cell formation **(Figure 2D supplemental**),
166 suggesting that the additional cells in the principal islet could also originate from the ducts.

167 We next tested the effect of CsA on endocrine progenitors in a regenerative context. We induced
168 regeneration in Tg(*neurod1:GFP*) larvae where the GFP is expressed in both endocrine progenitors and
169 mature endocrine cells. We first assessed generation of GFP cells at different time points (**Figure 2E**
170 **supplemental)** and showed that CsA induced an increase of neurod1+ cells from 4 dpt. The increase
171 was still detectable at least until 10dpt (**Figure 2E, Figure 2F supplemental**). To determine if these
172 additional cells result from their own proliferation, we performed a pulse of EdU just before analysis
173 (**Figure 2E supplemental**). We observed that CsA did not affect the neurod1+ cell proliferation rate
174 ,which is very low at these stages (**Figure 2F**). As a consequence, the effect of CsA cannot be explained
175 by endocrine cell proliferation but rather by neogenesis from progenitors. As CsA affects pro-endocrine
176 cells formation, we next wondered if the increased cell formation induced by CsA is specific to beta
177 cells. Treatment with CsA was performed as previously and delta1.1 and alpha cells were detected by
178 immunofluorescence. Interestingly, CsA did not affect alpha nor delta1.1 cells neogenesis in response
179 to beta cell ablation (**Figure 2G-H supplemental**). Overall, these experiments showed that CsA affects
180 specifically the beta cells and their endocrine progenitors.

181 *CaN over-activation abolishes the regenerative response*

182 We then wondered if an opposite regulation of CaN *i.e.* its activation impacts as well the regenerative
183 response. To that end, we generated a transgenic line Tg(*hsp70:GFP-P2A-ppp3ccCA*) that allows
184 ubiquitous expression of a constitutively active form of CaN^{CA} (*ppp3cc*^{CA}) upon heat shocks. Beta cell
185 ablation was triggered in Tg(*hsp70:GFP-P2A-ppp3cc*^{CA}); Tg(*ins:NTR-P2A-mCherry*); Tg(*nkx6.1:GFP*)
186 larvae from 3 to 4 dpf and CaN^{CA} expression was induced by four successive heat-shocks from 1 to 3
187 dpt (**Figure 3A**). The overexpression of CaN^{CA} after ablation impaired the regenerative response at 14
188 dpt (**Figure 3B-C**). Similar results were obtained with Tg(*UAS:GFP-P2A-ppp3cc*^{CA}); Tg(*cftr:gal4*)[45] ;
189 Tg(*ins:NTR-P2A-mCherry*) larvae in which CaN^{CA} is continuously and specifically overexpressed in the
190 ducts within the pancreas (**Figure 3D-E**). Importantly, the structure of the ducts was similar in CaN^{CA}
191 overexpressing larvae compared to Tg(*nkx6.1:GFP*) controls (**Figure 3D**), suggesting that the
192 suppression of the regenerative response in CaN^{CA}-overexpressing larvae was not due to

193 morphogenetic defects during ductal growth. This result shows that CaN acts directly in the ducts to
194 decrease beta cell regeneration while it is not necessary for normal beta cell differentiation.

195 *CaN regulates beta cell differentiation induced by Notch inhibition in absence of regeneration*

196

197 Our transcriptomic data showed that the Notch pathway is downregulated in ductal cells during beta
198 cell regeneration (**Figure 1**). As the level of Notch activity determines the behavior of ductal cells [33]
199 from quiescence to proliferation and subsequently to beta cell differentiation, we tested whether
200 calcineurin acts together with the Notch pathway on a common pool of ductal progenitors. To inhibit
201 the Notch pathway, we treated larvae with several concentrations of the gamma-secretase inhibitor
202 LY411575 from 3 to 4dpf in absence of regeneration. The activity of CaN was inhibited by CsA during
203 the same timeframe (**Figure 4A**). As previously, we used reporter lines for beta and ductal cells
204 *Tg*(*ins:NTR-P2A-mCherry*); *Tg*(*nkx6.1:GFP*) and the number of secondary beta cells was analyzed at
205 6dpf (**Figure 4A**). As expected, the number of beta cells progressively rose as the concentration of the
206 Notch inhibitor increased (**Figure 4B**). Combined treatment with CsA fostered the differentiation of
207 beta cells between 1 and 10 µM LY411575 but did not result in further increase at 15 µM LY411575
208 (**Figure 4B**), suggesting that CaN is important within a permissive window of Notch activity. Since we
209 overserved the highest synergistic effect at 5µM of LY411575, we used this concentration for the
210 following experiments (**Figure 4C-D**). It is worth noting that combined treatment of LY411575 (5uM)
211 and another CaN inhibitor, FK506, resulted in the same synergistic increase of beta cell differentiation
212 (**Figure 4A-B supplemental**), confirming that the effect is due to CaN inhibition. The combined effect
213 of Notch and CaN inhibition is transient as it is not observed at 7dpf anymore (**Figure 4E**). Therefore,
214 as observed in regenerative conditions (**Figure 2B**), CaN inhibition accelerates beta cell neogenesis
215 induced by Notch repression.

216 To determine to which extent CaN pathway can modulate Notch induced beta cell neogenesis, we
217 activated CaN^{CA} overexpression in *Tg*(*hsp70:GFP-P2A-ppp3cc*^{CA}*); Tg*(*ins:NTR-P2A-mCherry*) larvae by an
218 heat-shock at 3 dpf and treated them with LY411575 (**Figure 4C supplemental)**. CaN^{CA} overexpression
219 resulted in a lowered beta cell formation induced by Notch inhibition (**Figure 4D supplemental**),
220 revealing that CaN activation counterbalanced the effects of Notch inhibition. Using our previous
221 settings of Notch and CaN inhibition, we next wondered if the canonical pathway downstream of CaN
222 was involved in the enhancement of beta cell differentiation. To activate NFAT, a well-known target
223 of CaN, we used CHIR99021 allowing a stabilization of the active form of NFAT (**Figure 1D**). We found
224 that CHIR99021 rescued the effect of CsA (**Figure 4E supplemental**), suggesting that CaN inhibition
225 increases beta cell neogenesis at least partially by the regulation of NFAT. Overall, these results reveal
226 that CaN impacts beta cell formation in pro-endocrinogenic context, such as induced by a low level of

227 Notch activity. Moreover, it suggests that both CaN and Notch pathways act on a common pool of
228 ductal progenitors to govern beta cell neogenesis.

229

230 *CaN controls the proliferation of duct-associated progenitors induced by Notch inhibition*

231

232 Given that we observed the most significant increase in beta cell formation with CsA when Notch
233 activity was mildly repressed (**Figure 4B-D**), and since mild Notch activity has been shown to promote
234 progenitor amplification [35], it suggests that CaN acts at this level. To explore this possibility, we
235 exposed briefly *Tg*(*nkx6.1:GFP*) larvae to EdU after mild Notch (LY411575 5µM) and CaN inhibition
236 (**Figure 5A**) and analyzed at 4dpf and 6dpf. As expected, Notch inhibition increased the proportion of
237 proliferating EdU+ GFP+ duct cells at 4dpf (**Figure 5B-C**) and decreased the amount of ductal
238 progenitors 2 days later (at 6dpf) (**Figure 5D**), which is concomitant with the increase of beta cell
239 differentiation (**Figure 4C-D**). Interestingly, the combined inhibition with CsA further increased these
240 proportions, while CaN inhibition alone had no effect (**Figure 5B-D**). Of note, we detected beta cells
241 EdU+ at 6dpf (**Figure 5A supplemental**), underlying that these cells originate from the proliferation of
242 ductal progenitors.

243 Incidentally, at 4dpf, while the proliferation is increased (**Figure 5C**), the number of ductal cells
244 remained the same in all conditions (**Figure 5B supplemental**), suggesting that ductal cells have not
245 yet left the cell cycle to differentiate. In comparison, after stronger Notch inhibition (15µM), the ductal
246 cells are already depleted at 4dpf (**Figure 5C supplemental**), as they directly differentiate without
247 entering the cell cycle [35]. In these conditions, CsA could therefore not enhance ductal progenitor
248 proliferation and thus beta cell formation (**Figure 4B**). These results show that CaN and Notch
249 pathways act together on the proliferation of the ductal progenitors to prevent their exhaustion.

250 *CaN prevents exhaustion of Notch responsive progenitors during beta cell regeneration*

251

252 Taken together, our results indicate that CaN plays a role in the proliferation of ductal progenitors in
253 contexts that are permissive for beta cell differentiation. To demonstrate that CaN acts on ductal
254 progenitor proliferation in a similar manner to Notch inhibition but during regeneration, we exposed
255 *Tg(ins:NTR-P2A-mCherry*); *Tg(nkx6.1:GFP*) larvae after ablation and CsA treatment (**Figure 5E**). CaN
256 inhibition enhanced the proliferation of ductal cells in ablated larvae (**Figure 5F-G**). To next determine
257 if CaN acts on the Notch-responsive progenitors in beta cell regeneration, we then used
258 *Tg(tp1:VenusPest)* Notch reporter line. At larval stages the vast majority of ductal cells are Notch

259 responsive and the reporter line marks all the progenitors within the ductal tree [34]. We treated
260 *Tg(ins:NTR-P2A-mCherry*); *Tg(tp1:VenusPest)* as described above (**Figure 5E**). In ablated-larvae, CsA
261 increased tp1+ ductal cell proliferation (**Figure 5H-I**). Moreover, CsA induced a reduction of tp1+ ductal
262 cells in ablated larvae (**Figure 5 H-J**), suggesting an exhaustion of the Notch responsive progenitors, in
263 accordance with premature beta cell differentiation we observed (**Figure 2B-4D**). Lastly, CsA does not
264 affect tp1+ cells in non-ablated larvae showing that CaN inhibition did not directly affect Notch
265 signaling (**Figure 5J**). Those results suggest that CaN fine tunes the balance between proliferation of
266 the progenitors and their differentiation to prevent their exhaustion during beta cell regeneration.

267 *CaN regulation is functionally relevant in adult zebrafish*

268 To further expand upon our findings and investigate their relevance in a non-developmental context,
269 we next ought to determine whether CaN function is maintained in older zebrafish. We used 2 months
270 old *Tg*(*ins:NTR-P2A-mCherry*); *Tg*(*nkx6.1:GFP*) juveniles fish to perform beta cell ablation followed by
271 CsA treatments. We analyzed the number of small islets (up to 5 cells) at 7 and 10dpt. At 7dpt, CsA
272 increased the number of small islets in ablated juveniles (**Figure 6A-B**) showing that CaN inhibition
273 enhances beta cell regeneration in juvenile zebrafish, as in larvae. It is noteworthy that, as in larvae,
274 we highlighted an acceleration of beta cell regeneration. The increase number of small islets is indeed
275 transient as it not observe anymore at 10dpt (**Figure 6C**).

276 Next, we determined the functional impact of CaN overexpression or inhibition by assessing the
277 glycemia at 7, 10 and 14 after beta cell ablation. Overexpression of CaN^{CA} using either *Tg(hsp70:GFP-*
278 *P2A-ppp3cc*^{CA}*)* or *Tg*(*cftr:gal4*); *Tg*(*UAS:GFP-P2A-ppp3cc*^{CA}*),* led to an increased glycemia at both 7 and
279 10dpt (**Figure 6D-E)***,* before recovery at 14 dpt (**Figure 6A supplemental**). This indicates that the
280 overexpression of CaN delayed glycemia recovery induced by beta cell regeneration. However, CaN
281 inhibition did not seem to further improve the glycemia (**Figure 6D-E**) probably because the glycemia
282 was already low at 7dpt (77 mg/dL on average) compared to non-ablated control (50 mg/dl on average)
283 (**Figure 6D-E**). Altogether, these results show that in adult zebrafish also, CaN regulation is necessary
284 to enable beta cell regeneration and for proper recovery of the glycemia after beta cell loss.

285 **Discussion**

286 The present study reveals the importance of the protein phosphatase CaN as a new player in beta cell
287 regeneration in zebrafish. We demonstrate that CaN acts on ductal-associated progenitor cells by
288 balancing proliferation and endocrine differentiation. In addition, we show the interplay between CaN
289 and Notch signalling, a master regulator of beta cell regeneration.

290 Previous drug and genetic screening using zebrafish larvae enabled the identification of several
291 regulators of beta cell regeneration from different pancreatic cellular sources. For example, adenosine
292 has been shown to stimulate beta cell replication [28], igfbp1a [43] and TGFb suppression [30] promote
293 alpha-to-beta cell transdifferentiation. As for cdk5 inhibition and folinic acid/Folr1, they promote beta
294 cell regeneration from the pancreatic ducts [44], [45]. Here, to identify novel regulators of beta cell
295 regeneration specifically from pancreatic ducts, we carried out a transcriptomic profiling of duct cells
296 following beta cell ablation in the adult zebrafish. Transcriptomic analyses show that the regulated
297 genes encompass most of the genes and pathways identified in previous studies (igfbp1, mTor, Notch,
298 etc.), underlying the importance of those actors in beta cell regeneration. Our data reveal also that
299 DNA replication is the most enriched signature attesting that duct cells undergo a potent proliferative
300 response after the destruction of beta cells.

301 Besides these expected signatures, our transcriptomic data uncover the unanticipated upregulation of
302 numerous genes implicated in DNA repair and cell cycle arrest. These signatures might indicate that
303 highly proliferating ductal cells activate counteracting mechanisms. Among the genes regulated in
304 those signatures, we focused on CaN and determined its role in beta cell regeneration.
305 Pharmacological inhibition of CaN increases the proliferation of duct cells induced by beta cell ablation,
306 resulting in an acceleration of beta cell regeneration in the ducts. Consistently, transgene-mediated
307 CaN overactivation abolishes the regenerative response. Importantly, the inhibition of regeneration is
308 observed when CaN is overexpressed either ubiquitously or selectively in *cftr*-expressing ductal cells
309 indicating that the role of CaN in beta cell regeneration is intrinsic to the ducts. Based on functional
310 assays in larvae, we not only confirm the activation of the proliferation of ductal cells soon after beta
311 cell ablation, but also that the rate of progenitor proliferation is carefully controlled by CaN in order to
312 achieve proper and timely regeneration of beta cells. Our data are consistent with earlier studies
313 reporting a role of CaN in proliferation dynamics during fin regeneration. In the regenerating fin, low
314 CaN activity is found in the proximal region of the blastema characterized by a high rate of proliferation
315 and regeneration and its activity increases distally where lower proliferation is observed [36], [38],
316 [39]. It was suggested that CaN control blastemal cell progeny divisions [36]. In human, the importance
317 of CaN in proliferation is also highlighted in organ transplanted patients. When patients are treated
318 with Cyclosporin A (*i.e.* the CaN inhibitor we used in this study) as immunosuppressive drug they
319 indeed present an increased risk of skin cancer, notably due to keratinocyte senescence inhibition [46].

320 It has been shown that Notch inhibitory treatments switch progenitors from proliferative self-renewing
321 to premature differentiation, leading to progenitor depletion [34], [35]. Our study reveals that this
322 phenomenon is further exacerbated by CaN inhibition. Importantly, during normal larval development
323 in absence of Notch inhibitory treatment, CaN does not affect basal ductal proliferation nor beta cell

differentiation. Hence, Notch signalling has to be repressed to detect the effect of CaN on the progenitors, suggesting that CaN acts downstream of Notch pathway. In differentiating keratinocytes, CaN cooperates with Notch signalling to regulate p21/*cdkn1a* (which is upregulated in the ducts at 3 dpt), cell cycle withdrawal and differentiation [47]. These studies show that CaN acts in association with Notch signalling on progenitors proliferation and on their differentiation.

Based on our data, we build the model depicted in **Figure 7A**. Our study suggests that CaN acts in competent progenitor cells and that this competence is determined by Notch signalling. When Notch is repressed to a mild level, the progenitor enter into the cell cycle and acquire a pro-endocrinogenic competence [35]. CaN acts on these progenitors to tone down an excessive proliferation and avoid the exhaustion of these progenitors. CaN is therefore a guardian of the progenitor population. CaN inhibition both increases progenitor proliferation and induces their depletion, suggesting a switch to a symmetric division resulting in two daughter cells entering in endocrine differentiation.

More precisely, a previous study in mice uncover the existence of three division modes of the pancreatic progenitors during embryonic development, *i.e.* symmetric self-renewing resulting in two progenitors cells ; asymmetric resulting in a progenitor and a endocrine cell and symmetric differentiative resulting in two differentiated cells [48]. The authors actually show that the type of division is defined by the timing of induction of endocrine program by NEUROG3 [48]. Interestingly, NEUROG3 seems to be the link between proliferation and differentiation, and its expression is regulated by Notch signalling [49]. In zebrafish, endocrine differentiation is not induced by *Neurog3* but by *Ascl1b* and *Neurod1* [50]. Concerning that subject, CaN inhibition accelerates the formation of neurod1+ cells. Hence CaN could possibly act via the determination of the type of division *i.e.* symmetric vs asymmetric. This model is supported by previous observation in others systems. In stem cells and neuronal and hematopoietic progenitors, premature differentiation results from a switch in the mode of cellular division, from symmetric amplifying division to asymmetric differentiating division [51], [52]. Notch determines the choice between both types of divisions [53], [54].

Calcineurin is known to be implicated in cellular senescence [46]. Usually thought as negative regulators of development and cellular growth, DNA repair [55] and cellular senescence [56] appear to be required in both developmental and regenerative processes. Our transcriptomic data suggest that these mechanisms are required for beta cell regeneration. Therefore, it would be interesting to determine the contribution of these cellular processes in the ductal progenitors and determine if CaN acts via cellular senescence in this case.

Overall, this study brings new insights on beta cell regeneration and highlights the ductal progenitor cell cycle as a cornerstone in the process. Some studies report an increase of proliferation of some

ductal cell population in diabetic patients [10], [57], implying a regenerative response. However, these ductal cells cannot efficiently reform the beta cell mass, suggesting a dormant mechanism of regeneration. As such, the balance between proliferation and induction of endocrine differentiation could be a key to improve beta cell neogenesis. However, as CaN is also important for beta cell function, this approach would require to be transient to induce neogenesis. Therefore, it should be combined with methods to induce beta cell proliferation to ultimately reconstitute the beta cell mass. Overall, this study brings a better understanding on the regulation of the balance between ductal progenitors proliferation and endocrine differentiation. These results should provide new hints to help improve regenerative competences in mammals.

Material and Methods

Key resources table

Reagent type or resource	Designation	Source or reference	Identifier	Additional information
Genetic reagent (Danio rerio)	*TgBAC(nkx6.1:eGFP)^{ulg004}*	PMID: 26329351	ZFIN: ZDB-ALT-160205-1	
Genetic reagent (Danio rerio)	*Tg(ins:NTR-P2A-mCherry)^{ulg034}*	PMID: 29663654	ZFIN: ZDB-ALT-171122-9	
Genetic reagent (Danio rerio)	*Tg(cftr:gal4)*	PMID: 25592226	ZFIN : ZDB-FISH-150901-25442	
Genetic reagent (Danio rerio)	*Tg(tp1:VenusPest)*	PMID: 22492351	ZFIN: ZDB-FISH-150901-8023	
Genetic reagent (Danio rerio)	*Tg(hsp70:eGFP-P2A-ppp3ccaCA) ^{ulg068}*	This paper		See Zebrafish husbandry and generation of the *Tg(hsp70:eGFP-P2A-ppp3ccaCA) zebrafish line*
Genetic reagent (Danio rerio)	*Tg(UAS:eGFP-P2A-ppp3ccaCA) ^{ulg069}*	This paper		See Zebrafish husbandry and generation of the *Tg(UAS:eGFP-P2A-ppp3ccaCA) zebrafish line*
Antibody	Anti-GFP (chicken polyclonal)	Aves Labs	GFP-1020	1:1000

Antibody	anti-mCherry/dsRed (Living Colors Polyclonal)	Clontech	632496	1:500
Antibody	Anti-glucagon (mouse polyclonal)	Sigma	G2654	1:300
Antibody	Goat anti-Chicken IgY (H+L), Alexa Fluor™ 488	Invitrogen	A-11039	1:750
Antibody	Goat anti-dsred 568	Invitrogen		1:750
Antibody	Goat anti-Mouse IgG (H+L) Cross-Adsorbed Secondary Antibody, Alexa Fluor 633	Invitrogen		1:750
Chemical compound	Nifurpirinol (NFP)	Sigma-Aldrich	32439	
Chemical compound	Metronidazole (MTZ)	Sigma-Aldrich	M1547	
Chemical compound	Cyclosporine A (CsA)	Selleckchem	S2286	
Chemical compound	LY411575	Sigma-Aldrich	SML0506	
Chemical compound	CHIR990211	Sellekchem	CT99021	
Commercial assay or kit	Gateway™ LR Clonase™ II Enzyme mix	Invitrogen	11791020	
Commercial assay or kit	Gateway™ BP Clonase™ II Enzyme mix	Invitrogen	11789020	
Sequence based reagent	IM369	This paper	PCR primer	gaagaaaaccccggtcctatgtcgacgaaagagccgaaag
Sequence based reagent	IM380	This paper	PCR primer	ccttacacattcccgtcagtgc
Sequence based reagent	IM371	This paper	PCR primer	CGGCTCTTTCGTCGACATAGGACCGGGGTTTTCTTCCACG
Sequence based reagent	O226	This paper	PCR primer	GCCACCATGGTGAGCAAGGGCGAGGA
Sequence based reagent	IM370	This paper	PCR primer	ttattagatcttatttctgatcacctcctt
Sequence based reagent	IM459	This paper	PCR primer	cacacgaattcgccgccaccATGGTGAGCAAGGGCGAG
Sequence based reagent	IM460	This paper	PCR primer	ggatcggtcgagatccttacGATCTTATTTCTGATCACCTCCTTACG
Sequence based reagent	IM457	This paper	PCR primer	GTAAGGATCTCGACCGATCCTG
Sequence based reagent	IM458	This paper	PCR primer	GGTGGCGGCGAATTCGTG

Commercial assay or kit	Nextera® XT DNA Library kit	Illumina	FC-131-1024	
Commercial assay or kit	Click-iT™ EdU Cell Proliferation Kit for Imaging, Alexa Fluor™ 647 dye	Invitrogen	C10340	
Software, algorithm	Imaris	Bitplane (http://www.bitplane.com/imaris/imaris)	RRID:SCR_007370	Version 9.5
Software, algorithm	GraphPad Prism	GraphPad Prism (https://graphpad.com)	RRID:SCR_015807	Version 8
Software, algorithm	DESeq2	DESeq2 (https://bioconductor.org/packages/release/bioc/html/DESeq2.html)	RRID:SCR_015687	
Software, algorithm	WebGestalt	WebGestalt (http://www.webgestalt.org/)	RRID:SCR_006786	

Zebrafish husbandry and generation of the Tg(hsp70:eGFP-P2A-ppp3ccaCA)^{ulg068} and Tg(UAS:eGFP-P2A-ppp2ccaCA)^{ulg069} zebrafish lines

Tg BAC(nkx6.1:eGFP)^{ulg004} [58] *; Tg(ins:NTR-P2A-mCherry)^{ulg034}* [59] *; Tg(cftr:gal4)* and *Tg(tp1:VenusPest)* were used. Zebrafish were raised in standard conditions at 28°C. All experiments were carried out in compliance with the European Union and Belgian law and with the approval of the ULiège Ethical Committee for experiments with laboratory animals (approval number : 2075).

The *hsp70:GFP-P2A-ppp3ccaCA* transgene has been generated by cloning a PCR fragment containing the Gateway vector pCR8/GW/TOPO. Firstly, we amplified the full length of ppp3ccaCA with primers IM369/IM380 and amplified *GFP-P2A* with overlapping regions with IM371/O226. The overlapping PCR used the primers O226/IM380. Then to obtain a truncated *ppp3ccaCA* lacking the calmodulin biding and the autoinhibitory domain, resulting in a constantly active form of calcineurin, we amplified the last fragments with IM370/O226 and cloned into PCR8 vector. The promoter was assembled by LR recombination with pE5-hsp70 into pDestTol2p2A from the Tol2kit [60]. *Tg (hsp70:GFP-P2A-ppp3ccaCA)* fish have been generated using the Tol2 mediated transgenesis [61]. *The Tg(UAS:GFP-*

385 *P2A-ppp3ccacA*) has been generated by ligation (KLD kit, NEB) of PCR fragments *GFP-P2A-ppp3ccacA*
386 *(*IM459/IM460) with the UAS sequences (IM457/IM458) in plasmid from (Distel 2009) and then
387 inserted into pDestTol2p2A from the Tol2kit. Final constructions has been injected with transposase
388 into wild type (WT) AB embryos.
389
390 *Beta-cell ablation*

391 Adults fish for RNA-sequencing experiment were treated with freshly prepared metronidazole (MTZ)
392 (Sigma M1547) at 10mM with 0.2% DMSO in fish water. Control treatments consisted of fish water
393 containing 0.2% DMSO. Fish were treated for 18 hours in the dark. Nifurpirinol (NFP) (32439, Sigma-
394 Aldrich) stock solution was dissolved at 2.5 mM in DMSO. b-cell ablation in *Tg(nkx6.1:eGFP);*
395 *Tg(ins:NTR-P2A-mCherry)* larvae was induced by treatment with 2.5 µM NFP in E3. Control treatments
396 consisted of E3 containing 0.2% DMSO. Larvae were treated for 18 hours in the dark.

397 *Drug treatments*

398 Cyclosporine A (Selleckchem, S2286), CHIR99021 and LY411575 (Sigma-Aldrich, SML0506) stock
399 solution were dissolved at 10mM in DMSO. Larvae treatment were respectively performed at 0.1 µM
400 and 5µM in E3. Control treatments consisted of E3 containing the same amount of DMSO than drug
401 treatment. Larvae were treated for 18 hours in the dark.

402 *5-ethynyl-2'-deoxyuridine (EdU) incorporation assay*

403 Zebrafish larvae were incubated in 4 mM EdU dissolved in E3 water for 8 hours, they were then directly
404 euthanised in tricaine and fixed in 4% PFA. EdU was detected according to the protocol of Click-iT™
405 EdU Cell Proliferation Kit for Imaging, Alexa Fluor™ 647 (ThermoFisher C10340) after whole mount
406 immunodetection.

407 *Heat Shock*

408 *Successive heat shocks of 30 minutes and 12 hours apart were performed at 39°C for larvae and 37°C*
409 *for juveniles and adults zebrafish.*

410 *Whole mount immunodetection*

411 Larvae were euthanized in tricaine and fixed in 4% PFA at 4 °C for IHC. The digestive tract of juveniles
412 was dissected prior immunodetection and kept in methanol for at least 18 hours. After depigmentation
413 with 3% H2O2/1% KOH, larvae were permeabilised 30 min in PBS/ Triton X-100 and incubated for two
414 hours in blocking buffer (4% goat serum/1% BSA/PBS/0.1% Triton X-100). Primary and secondary
415 antibodies were incubated at 4 °C overnight.

	Fixation duration	Depigmentation duration	Permeabilization solution	Permeabilization duration
5-10 dpf	18 hours	15 min	PBTr 0.05%	30 min
13-17 dpf	36 hours	20 min	PBTr 2%	30 min
2months (digestive tract)	18 hours	15 min	/	/

416

417 Primary antibodies: Living Colors Polyclonal anti-mCherry/dsRed (rabbit, 1:500, Clontech 632496),
418 anti-GFP (chicken, 1:1000),

419 Secondary antibodies: Alexa Fluor-488, -568, -633 (goat, 1:750, Molecular Probes).

420 *Flow cytometry and FACS*

421 The whole pancreas from 3-4 fish of *Tg(nkx6.1:eGFP); Tg(ins:NTR-P2A-mCherry)* adult fish (6–10
422 months old, males and females) were dissected, collected and washed in HBSS without Ca^{2+}/Mg^{2+}. Live
423 cell dissociation was performed in Tryple Select 1x solution (GIBCO) supplemented with 100 U/mL
424 collagenase IV (Life Technologies 17104-019) and 40 µg/mL proteinase K (Invitrogen, 25530031) for 10
425 min at 28 °C.

426 The GFP+ cells were selected on FACS Aria III and sorted under purity mode and after exclusion of the
427 doublets. The purity of the sorted cells was confirmed by epifluorescence microscopy (~95 %). Cells
428 (about 1000-5000/fish depending on the cell type) were immediately lysed with 0.5% Triton X-100
429 containing 2U/µl RNAse inhibitor and stored at –80 °C.

430 *mRNA sequencing of FACSed cells and bioinformatic analyses*

431 cDNAs were prepared from lysed cells according to SMART-Seq2.0 (Picelli et al., 2014) for low input
432 RNA sequencing and libraries were prepared with Nextera® DNA Library kit (Illumina). Independent
433 biological replicates of each cell type sequenced using Illumina NextSeq500 and obtained ~20 million
434 100 bp paired-end reads. Reads were mapped and aligned to the zebrafish genome GRCz11 from
435 Ensembl gene annotation version using STAR version 2.6.1 (Dobin et al., 2013). Gene expression levels
436 were calculated with featureCounts (http://bioinf.wehi.edu.au/featureCounts/) and differential
437 expression determined with DESeq2 (Love, Huber, & Anders, 2014). Expression values are given as
438 normalized read counts. Poorly expressed genes with mean normalized expression counts <10 were
439 excluded from the subsequent analyses. DESeq2 uses Wald test for significance with posterior
440 adjustment of P values (Padj) using Benjamini and Hochberg multiple testing. The differentially
441 expressed (DE) genes identified with a Padj cutoff of 0.05 were submitted for GO analysis using
442 WebGestalt tool (Liao, Wang, Jaehnig, Shi, &Zhang, 2019).

443 *Confocal microscopy and image analysis*

444 Images were acquired using Leica SP5 confocal microscope. We used ImageJ to count the cells and
445 Imaris to do the pictures.

446 *Glycemia measurement*

447 *Glycemia measurement were performed as described in* [59].

448 **Data availability**

449 The sequences that support the findings are of this study have been deposit in Geo with the accessions
450 codes GSE212124, https://www.ncbi.nlm.nih.gov/geo/info/linking.html. The authors declare that all
451 other data supporting the findings of this study are available within the paper and its supplementary
452 information files.

453 **Authors contribution**

454 **L.M.** conducted experiments, acquired and analysed data, analysed transcriptomic data, wrote the
455 manuscript. **D.B.** conducted RNA-seq experiment and revised the manuscript **A.L.** implemented
456 bioinformatic programs and analysed transcriptomic data. **C.R., C.G. and C.D.** conducted experiments.
457 **L.F.** revised the manuscript. **B.P.** provided resources and advised on research studies. **M.L.V.** provided
458 resources, advised on research studies and revised the manuscript **I.M.** supervised the whole work,
459 acquired funding, designed the research studies, verified data and assisted in writing the manuscript.

460 **Acknowledgments**

461 The authors thank the EOS (Excellence of Sciences) program from FNRS and more especially Dr.
462 Emmanuel Dejardin for support. We also thank the GIGA technology platforms, GIGA-Genomics and
463 GIGA-Imaging. The authors also thanks Jérémie Zappia for critically reading the manuscript, Jordane
464 Bourdouxhe and Marie Alice Dupont for their help with the constructions.

465 **Duality of interest**

466 No potential conflicts of interest.

467 **References**

468 [1] Y. Dor, J. Brown, O. I. Martinez, and D. a Melton, "Adult pancreatic beta-cells are formed by
469 self-duplication rather than stem-cell differentiation.," *Nature*, vol. 429, no. model 3, pp. 41–
470 46, 2004, doi: 10.1038/nature02520.

471 [2] F. Thorel *et al.*, "Conversion of Adult Pancreatic alpha-cells to Beta-cells after Extreme Beta
472 Cell Loss," *Nature*, vol. 464, no. 7292, pp. 1149–1154, 2010, doi:
473 10.1038/nature08894.Conversion.

474 [3] S. Chera *et al.*, "Diabetes recovery by age-dependant conversion of pancreatic delta-cells into
475 insulin producers," *Nature*, vol. 514, no. 7523, pp. 503–507, 2014, doi:

476 10.1038/nature13633.Diabetes.

477 [4] X. Xu *et al.*, “Beta Cells Can Be Generated from Endogenous Progenitors in Injured Adult
478 Mouse Pancreas,” *Cell*, vol. 132, pp. 197–207, 2008, doi: 10.1016/j.cell.2007.12.015.

479 [5] M. Solar *et al.*, “Pancreatic Exocrine Duct Cells Give Rise to Insulin-Producing β Cells during
480 Embryogenesis but Not after Birth,” *Dev. Cell*, vol. 17, pp. 849–860, 2009, doi:
481 10.1016/j.devcel.2009.11.003.

482 [6] H. Zhao *et al.*, “Pre-existing beta cells but not progenitors contribute to new beta cells in the
483 adult pancreas,” *Nat. Metab.*, vol. 3, no. 3, pp. 352–365, 2021, doi: 10.1038/s42255-021-
484 00364-0.

485 [7] J. L. Kopp *et al.*, “Sox9+ ductal cells are multipotent progenitors throughout development but
486 do not produce new endocrine cells in the normal or injured adult pancreas,” *Development*,
487 vol. 138, pp. 653–665, 2011, doi: 138/4/653 [pii].

488 [8] M. Courtney *et al.*, “The Inactivation of Arx in Pancreatic α-Cells Triggers Their Neogenesis and
489 Conversion into Functional β-Like Cells,” *PLoS Genet.*, vol. 9, no. 10, pp. 1–18, 2013, doi:
490 10.1371/journal.pgen.1003934.

491 [9] C. Gribben *et al.*, “Ductal Ngn3-expressing progenitors contribute to adult β cell neogenesis in
492 the pancreas,” *Cell Stem Cell*, vol. 28, no. 11, pp. 2000-2008.e4, 2021, doi:
493 10.1016/j.stem.2021.08.003.

494 [10] M. M. F. Qadir *et al.*, “Single-cell resolution analysis of the human pancreatic ductal
495 progenitor cell niche,” *Proc. Natl. Acad. Sci. U. S. A.*, vol. 117, no. 20, pp. 10876–10887, 2020,
496 doi: 10.1073/pnas.1918314117.

497 [11] J. B. Moss, P. Koustubhan, M. Greenman, M. J. Parsons, I. Walter, and L. G. Moss,
498 “Regeneration of the pancreas in adult zebrafish,” *Diabetes*, vol. 58, no. August, pp. 1844–
499 1851, 2009, doi: 10.2337/db08-0628.

500 [12] K. D. Poss, L. G. Wilson, and M. T. Keating, “Heart regeneration in zebrafish,” *Science (80-.).*,
501 vol. 298, no. 5601, pp. 2188–2190, 2002, doi: 10.1126/science.1077857.

502 [13] T. Y. Choi, N. Ninov, D. Y. R. Stainier, and D. Shin, “Extensive conversion of hepatic biliary
503 epithelial cells to hepatocytes after near total loss of hepatocytes in zebrafish,”
504 *Gastroenterology*, vol. 146, no. 3, pp. 776–788, 2014, doi: 10.1053/j.gastro.2013.10.019.

505 [14] Y. Goldshmit, T. E. Sztal, P. R. Jusuf, T. E. Hall, M. Nguyen-Chi, and P. D. Currie, “Fgf-dependent

506 glial cell bridges facilitate spinal cord regeneration in zebrafish.," *J. Neurosci.*, vol. 32, no. 22,
507 pp. 7477–7492, May 2012, doi: 10.1523/JNEUROSCI.0758-12.2012.

508 [15] V. Kroehne, D. Freudenreich, S. Hans, J. Kaslin, and M. Brand, "Regeneration of the adult
509 zebrafish brain from neurogenic radial glia-type progenitors," *Development*, vol. 138, no. 22,
510 pp. 4831–4841, 2011, doi: 10.1242/dev.072587.

511 [16] M. Gemberling, T. J. Bailey, D. R. Hyde, and K. D. Poss, "The zebrafish as a model for complex
512 tissue regeneration," *Trends Genet.*, vol. 29, no. 11, pp. 611–620, 2013, doi:
513 10.1016/j.tig.2013.07.003.

514 [17] C. Papadimitriou *et al.*, "3D Culture Method for Alzheimer's Disease Modeling Reveals
515 Interleukin-4 Rescues Aβ42-Induced Loss of Human Neural Stem Cell Plasticity," *Dev. Cell*, vol.
516 46, no. 1, pp. 85-101.e8, 2018, doi: 10.1016/j.devcel.2018.06.005.

517 [18] V. Mashkaryan *et al.*, "Type 1 Interleukin-4 Signaling Obliterates Mouse Astroglia in vivo but
518 Not in vitro," *Front. Cell Dev. Biol.*, vol. 8, no. February, pp. 1–16, 2020, doi:
519 10.3389/fcell.2020.00114.

520 [19] S. Ko, T. Choi, J. O. Russell, J. So, and D. Shin, "Bromodomain and extraterminal (BET) proteins
521 regulate biliary-driven liver regeneration," *J. Hepatol.*, vol. 64, no. 2, pp. 316–325, 2016, doi:
522 10.1016/j.jhep.2015.10.017.Bromodomain.

523 [20] Y. Goldshmit *et al.*, "Decreased anti-regenerative effects after spinal cord injury in spry4-/-
524 mice.," *Neuroscience*, vol. 287, pp. 104–112, Feb. 2015, doi:
525 10.1016/j.neuroscience.2014.12.020.

526 [21] B. V. Fausett, J. D. Gumerson, and D. Goldman, "The proneural basic helix-loop-helix gene
527 Ascl1a is required for retina regeneration," *J. Neurosci.*, vol. 28, no. 5, pp. 1109–1117, 2008,
528 doi: 10.1523/JNEUROSCI.4853-07.2008.

529 [22] L. Massoz, M. A. Dupont, and I. Manfroid, "Zebra-fishing for regenerative awakening in
530 mammals," *Biomedicines*, vol. 9, no. 1, pp. 1–18, 2021, doi: 10.3390/biomedicines9010065.

531 [23] H. Pisharath, "Validation of nitroreductase, a prodrug-activating enzyme, mediated cell death
532 in embryonic zebrafish (Danio rerio)," *Comp. Med.*, vol. 57, no. 3, pp. 241–246, 2007.

533 [24] S. Curado, R. M. Anderson, B. Jungblut, J. Mumm, E. Schroeter, and D. Y. R. Stainier,
534 "Conditional targeted cell ablation in zebrafish: A new tool for regeneration studies," *Dev.
535 Dyn.*, vol. 236, no. February, pp. 1025–1035, 2007, doi: 10.1002/dvdy.21100.

536 [25] H. Pisharath, J. M. Rhee, M. a Swanson, S. D. Leach, and M. J. Parsons, "Targeted ablation of
537 beta cells in the embryonic zebrafish pancreas using E.coli nitroreductase," *Mech Dev.*, 2007,
538 doi: 10.1016/j.mod.2006.11.005.Targeted.

539 [26] F. Delaspre *et al.*, "Centroacinar cells are progenitors that contribute to endocrine pancreas
540 regeneration," *Diabetes*, vol. 64, no. October, pp. 3499–3509, 2015, doi: 10.2337/db15-0153.

541 [27] A. P. Ghaye *et al.*, "Progenitor potential of nkx6.1-expressing cells throughout zebrafish life
542 and during beta cell regeneration," *BMC Biol.*, vol. 13, p. 70, 2015, doi: 10.1186/s12915-015-
543 0179-4.

544 [28] O. Andersson *et al.*, "Adenosine signaling promotes regeneration of pancreatic β- cells in
545 vivo," *Cell Metab.*, 2012, doi: 10.1016/j.cmet.2012.04.018.Adenosine.

546 [29] L. Ye, M. A. Robertson, D. Hesselson, D. Y. R. Stainier, and R. M. Anderson, "Glucagon is
547 essential for alpha cell transdifferentiation and beta cell neogenesis," *Dev.*, vol. 142, no. 8, pp.
548 1407–1417, 2015, doi: 10.1242/dev.117911.

549 [30] C. S. M. Helker *et al.*, "A whole organism small molecule screen identifies novel regulators of
550 pancreatic endocrine development," *Dev.*, vol. 146, no. 14, 2019, doi: 10.1242/dev.172569.

551 [31] C. Carril Pardo *et al.*, "A delta-cell subpopulation with a pro-beta-cell identity contributes to
552 efficient age-independent recovery in a zebrafish model of diabetes," *Elife*, 2022.

553 [32] S. P. Singh *et al.*, "A single-cell atlas of de novo β-cell regeneration reveals the contribution of
554 hybrid β/δ-cells to diabetes recovery in zebrafish," *Development*, vol. 149, no. 2, 2022, doi:
555 10.1242/dev.199853.

556 [33] N. Ninov, D. Hesselson, P. Gut, A. Zhou, K. Fidelin, and D. Y. R. Stainier, "Metabolic regulation
557 of cellular plasticity in the pancreas," *Curr. Biol.*, vol. 23, no. 13, pp. 1242–1250, 2013, doi:
558 10.1016/j.cub.2013.05.037.

559 [34] M. J. Parsons *et al.*, "Notch-responsive cells initiate the secondary transition in larval zebrafish
560 pancreas," *Mech. Dev.*, vol. 126, no. 10, pp. 898–912, 2009, doi: 10.1016/j.mod.2009.07.002.

561 [35] N. Ninov, M. Borius, and D. Y. R. Stainier, "Different levels of Notch signaling regulate
562 quiescence, renewal and differentiation in pancreatic endocrine progenitors," *Development*,
563 vol. 139, no. 9, pp. 1557–1567, 2012, doi: 10.1242/dev.076000.

564 [36] V. A. Tornini *et al.*, "Live Monitoring of Blastemal Cell Contributions During Appendage
565 Regeneration," *Curr. Biol.*, 2016, doi: 10.1016/j.cub.2016.08.072.Live.

566 [37] S. C. McMillan *et al.*, “A regulatory pathway involving retinoic acid and calcineurin demarcates
567 and maintains joint cells and osteoblasts in regenerating fin,” *Dev.*, vol. 145, no. 11, 2018, doi:
568 10.1242/DEV.161158.

569 [38] Z. Cao *et al.*, “Calcineurin controls proximodistal blastema polarity in zebrafish fin
570 regeneration,” *Proc. Natl. Acad. Sci. U. S. A.*, vol. 118, no. 2, pp. 2–9, 2021, doi:
571 10.1073/pnas.2009539118.

572 [39] S. Kujawski *et al.*, “Calcineurin Regulates Coordinated Outgrowth of Zebrafish Regenerating
573 Fins,” *Dev. Cell*, vol. 28, no. 5, pp. 573–587, 2014, doi: 10.1016/j.devcel.2014.01.019.

574 [40] E. Tarifeño-Saldivia *et al.*, “Transcriptome analysis of pancreatic cells across distant species
575 highlights novel important regulator genes,” *BMC Biol.*, vol. 15, no. 1, pp. 1–19, 2017, doi:
576 10.1186/s12915-017-0362-x.

577 [41] J. J. Heit *et al.*, “Calcineurin/NFAT signalling regulates pancreatic β-cell growth and function,”
578 *Nature*, vol. 443, no. 7109, pp. 345–349, 2006, doi: 10.1038/nature05097.

579 [42] J. Mi, K. C. Liu, and O. Andersson, “Decoding pancreatic endocrine cell differentiation and β
580 cell regeneration in zebrafish,” *Sci. Adv.*, vol. 9, no. 33, p. eadf5142, 2023, doi:
581 10.1126/sciadv.adf5142.

582 [43] J. Lu *et al.*, “ IGFBP 1 increases β-cell regeneration by promoting α- to β-cell
583 transdifferentiation ,” *EMBO J.*, vol. 35, no. 18, pp. 2026–2044, 2016, doi:
584 10.15252/embj.201592903.

585 [44] C. Karampelias *et al.*, “Reinforcing one-carbon metabolism via folic acid/Folr1 promotes β-cell
586 differentiation,” *Nat. Commun.*, vol. 12, no. 1, pp. 1–13, 2021, doi: 10.1038/s41467-021-
587 23673-0.

588 [45] K. C. Liu *et al.*, “Inhibition of Cdk5 promotes β-cell differentiation from ductal progenitors,”
589 *Diabetes*, vol. 67, no. 1, pp. 58–70, 2017, doi: 10.2337/db16-1587.

590 [46] X. Wu *et al.*, “Calcineurin and ATF3: opposite roles in squamous skin cancer,” *Nature*, 2010,
591 doi: 10.1038/nature08996.Calcineurin.

592 [47] C. Mammucari *et al.*, “Integration of notch 1 and calcineurin/NFAT signaling pathways in
593 keratinocyte growth and differentiation control,” *Dev. Cell*, vol. 8, no. 5, pp. 665–676, 2005,
594 doi: 10.1016/j.devcel.2005.02.016.

595 [48] Y. H. Kim, H. L. Larsen, P. Rué, L. A. Lemaire, J. Ferrer, and A. Grapin-Botton, “Cell Cycle–

596 Dependent Differentiation Dynamics Balances Growth and Endocrine Differentiation in the
597 Pancreas," *PLoS Biol.*, vol. 13, no. 3, 2015, doi: 10.1371/journal.pbio.1002111.

598 [49] N. A. J. Krentz *et al.*, "Phosphorylation of NEUROG3 Links Endocrine Differentiation to the Cell
599 Cycle in Pancreatic Article Phosphorylation of NEUROG3 Links Endocrine Differentiation to the
600 Cell Cycle in Pancreatic Progenitors," *Dev. Cell*, vol. 41, no. 2, pp. 129-142.e6, 2017, doi:
601 10.1016/j.devcel.2017.02.006.

602 [50] L. C. Flasse, D. G. Stern, J. L. Pirson, I. Manfroid, B. Peers, and M. L. Voz, "The bHLH
603 transcription factor Ascl1a is essential for the specification of the intestinal secretory cells and
604 mediates Notch signaling in the zebrafish intestine," *Dev. Biol.*, vol. 376, no. 2, pp. 187–197,
605 2013, doi: 10.1016/j.ydbio.2013.01.011.

606 [51] W. B. Huttner and Y. Kosodo, "Symmetric versus asymmetric cell division during neurogenesis
607 in the developing vertebrate central nervous system," *Curr. Opin. Cell Biol.*, vol. 17, no. 6, pp.
608 648–657, 2005, doi: 10.1016/j.ceb.2005.10.005.

609 [52] A. D. Ho and W. Wagner, "The beauty of asymmetry: Asymmetric divisions and self-renewal in
610 the haematopoietic system," *Curr. Opin. Hematol.*, vol. 14, no. 4, pp. 330–336, 2007, doi:
611 10.1097/MOH.0b013e3281900f12.

612 [53] R. S. Bultje, D. R. Castaneda-Castellanos, L. Y. Jan, Y. N. Jan, A. R. Kriegstein, and S. H. Shi,
613 "Mammalian Par3 Regulates Progenitor Cell Asymmetric Division via Notch Signaling in the
614 Developing Neocortex," *Neuron*, vol. 63, no. 2, pp. 189–202, 2009, doi:
615 10.1016/j.neuron.2009.07.004.

616 [54] M. Guo, L. Y. Jan, and Y. N. Jan, "Control of daughter cell fates during asymmetric division:
617 Interaction of Numb and Notch," *Neuron*, vol. 17, no. 1, pp. 27–41, 1996, doi: 10.1016/S0896-
618 6273(00)80278-0.

619 [55] K. Sousounis *et al.*, "Eya2 promotes cell cycle progression by regulating DNA damage response
620 during vertebrate limb regeneration," 2020.

621 [56] S. Da *et al.*, "Cell senescence contributes to tissue regeneration in zebrafish," no. July 2019,
622 pp. 1–5, 2020, doi: 10.1111/acel.13052.

623 [57] A. S. Md Moin, P. C. Butler, and A. E. Butler, "Increased proliferation of the pancreatic duct
624 gland compartment in type 1 diabetes," *J. Clin. Endocrinol. Metab.*, vol. 102, no. 1, pp. 200–
625 209, 2017, doi: 10.1210/jc.2016-3001.

626 [58] A. P. Ghaye *et al.*, "Progenitor potential of nkx6.1-expressing cells throughout zebrafish life

627 and during beta cell regeneration," *BMC Biol.*, vol. 13, no. 1, 2015, doi: 10.1186/s12915-015-
628 0179-4.

629 [59] D. Bergemann *et al.*, "Nifurpirinol: A more potent and reliable substrate compared to
630 metronidazole for nitroreductase-mediated cell ablations," *Wound Repair Regen.*, vol. 26, no.
631 2, pp. 238–244, 2018, doi: 10.1111/wrr.12633.

632 [60] K. M. Kwan *et al.*, "The Tol2kit: a multisite gateway-based construction kit for Tol2 transposon
633 transgenesis constructs.," *Dev. Dyn. an Off. Publ. Am. Assoc. Anat.*, vol. 236, no. 11, pp.
634 3088–3099, Nov. 2007, doi: 10.1002/dvdy.21343.

635 [61] K. Kawakami, "Tol2: a versatile gene transfer vector in vertebrates.," *Genome Biol.*, vol. 8
636 Suppl 1, p. S7, 2007, doi: 10.1186/gb-2007-8-s1-s7.

637

638 **Legends**

639

640 **Figure 1 :** *Transcriptomic profiling of ductal cells during beta cell regeneration and validation in larvae*

641 A-B) Enrichment ratio of selected non-redundant signatures of KEGG pathways overrepresented
642 in ductal cells after beta cells ablation (UP – A and DOWN -B) compared to ductal cells without
643 beta cells ablation. Gene Ontology (GO) terms were identified using ORA analysis by WebGestalt
644 (Liao et al., 2019) using the list of DE genes provided by DESeq. The light color for Notch pathway
645 means p-value = 0.11.

646 C) List of genes associated with the signature of cellular senescence from A-B. Genes related to
647 CaN pathway are in bold.

648 D) Calcineurin canonical pathway with up-regulated genes in green and down-regulated genes in
649 red in transcriptomic data from A-B.

650 E) Experimental design for regeneration test in larvae. Briefly, after nifurpirinol treatment from 3
651 to 4dpf, larvae were fixed and analyzed at 4-7-10 and 14 days post treatment (dpt).

652 F) Graph representing the mean number of mCherry+ beta cells in the pancreatic tail of *Tg(ins:NTR-*
653 *P2A-mCherry) ; Tg(nkx6.1:GFP)* at 0-4-7-10 and 14 dpt. The gray spheres represent non-ablated
654 conditions and the pink triangles the ablated condition. Data are presented as mean values ± SEM.
655 One-way ANOVA test with Tukey's multiple comparison test, ****p-value<0.0005.

656 G) Whole mount fluorescent immunohistochemistry (GFP and mCherry) of the pancreas of
657 *Tg(ins:NTR-P2A-mCherry) ; Tg(nkx6.1:GFP)* larvae at 14dpt. 3D projection (stack) of one non-
658 ablated and one ablated representative samples. The principal islet (PI) and the pancreatic tail are
659 shown. Arrows point out mCherry+ beta cells in the pancreatic tail. Scale 100µM.

660 H) Experimental design for EdU assay in larvae. After NFP treatment for 3 to 4dpf, larvae were
661 exposed to EdU at 2dpt before fixation for analysis.

662 I) Whole mount fluorescent immunohistochemistry (GFP and EdU) of the pancreatic tail of
663 *Tg(ins:NTR-P2A-mCherry) ; Tg(nkx6.1:GFP)* larvae at 2dpt. 3D projection (stack) of one non-ablated
664 and one ablated representative samples. Arrows point out GFP+ duct cells EdU+ in the pancreatic
665 tail. Scale 50µM.

666 J) Barplot representing the percentage of GFP+ ductal cells which incorporated EdU+ in non-
667 ablated and ablated conditions. Data are presented as mean values ± SD. T-test. **p-value<0.005.

668

669 **Figure 2 :** *Calcineurin inhibition with CsA increases the ductal regenerative response*

670 **A)** Experimental design for regeneration test in larvae with CsA treatment. Briefly, after
671 nifurpirinol treatment from 3 to 4dpf, larvae were treated with CsA from 1 to 3dpt and fixed
672 and analyzed at 4-7-10 and 14 days post treatment (dpt).
673 **B)** Graph representing the mean number of mCherry+ beta cells in the pancreatic tail of
674 *Tg(ins:NTR-P2A-mCherry) ; Tg(nkx6.1:GFP)* at 0-4-7-10 and 14 dpt. The gray spheres represent
675 non-ablated condition ; the pink triangles represent the ablated condition ; the black squares
676 CsA condition and inverted green triangles ablated + CsA condition. Data are presented as
677 mean values ± SEM. Two-way ANOVA test with Sidak's multiple comparisons test, *p-
678 value<0.05.
679 **C)** Whole mount fluorescent immunohistochemistry (GFP and mCherry) of the pancreas of
680 *Tg(ins:NTR-P2A-mCherry) ; Tg(nkx6.1:GFP)* larvae at 10dpt. 3D projection (stack) of non-
681 ablated and ablated larvae treated with DMSO or CsA representative samples. The principal
682 islet (PI) and the pancreatic tail are shown. Arrows point out mCherry+ beta cells in the
683 pancreatic tail. Scale 100µM.
684 **D)** Barplot representing the number of number of mCherry+ beta cells in the pancreatic tail of
685 *Tg(ins:NTR-P2A-mCherry) ; Tg(nkx6.1:GFP)* larvae at 10dpt. The gray spheres represent non-
686 ablated condition ; the pink triangles represent the ablated condition ; the black squares CsA
687 condition and inverted green triangles ablated + CsA condition. Data are presented as mean
688 values ± SD. Two-way ANOVA with Tukey's multiple comparison test, *p-value<0.05.
689 **E)** Graph representing the mean number of GFP+ neurod1+ cells in the pancreatic tail of
690 *Tg(ins:NTR-P2A-mCherry) ; Tg(neurod1:GFP)* at 0-4-7 and 10 dpt. The gray spheres represent
691 non-ablated condition ; the pink triangles represent the ablated condition ; the black squares
692 CsA condition and inverted green triangles ablated + CsA condition. Data are presented as
693 mean values ± SEM. Two-way ANOVA test with Sidak's multiple comparisons test, **p-
694 value<0.005; *** p-value<0.0005; **** p-value<0.00005.
695 **F)** Graph representing the mean number of GFP+ neurod1 EdU+ cells in the pancreatic tail of
696 *Tg(ins:NTR-P2A-mCherry) ; Tg(neurod1:GFP)* at 0-4-7 and 10 dpt. The gray spheres represent
697 non-ablated condition ; the pink triangles represent the ablated condition ; the black squares
698 CsA condition and inverted green triangles ablated + CsA condition. Data are presented as
699 mean values ± SEM.
700
701
702 **Figure 3:** *Transgenic mediated overexpression of calcineurin abolish the ductal regenerative response*
703
704 **A)** Experimental design for regeneration test in larvae with heat-shocks. Briefly, after nifurpirinol
705 treatment from 3 to 4dpf, four heat shock were performed from 1 to 3dpt and larvae were
706 fixed and analyzed at 14dpt.

707 **B)** Whole mount fluorescent immunohistochemistry (GFP and mCherry) of the pancreas of
708 *Tg(hsp70:CaN^{CA}); Tg(ins:NTR-P2A-mCherry); Tg(nkx6.1:GFP)* larvae at 14dpt. 3D projection
709 (stack) of one non-ablated and one ablated with or without heat-shock representative
710 samples. The principal islet (PI) and the pancreatic tail are showed. Arrows point out mCherry+
711 beta cells in the pancreatic tail. Scale 100µM.
712 **C)** Barplot representing the mean number of mCherry+ beta cells in the pancreatic tail of
713 *Tg(hsp70:CaN^{CA}); Tg(ins:NTR-P2A-mCherry); Tg(nkx6.1:GFP)* larvae at 14dpt. The gray spheres
714 represent non-ablated condition ; the pink triangles represent the ablated condition ; the black
715 squares heat-shock condition and inverted green triangles ablated + heat-shock condition.
716 Data are presented as mean values ± SD. Two-way ANOVA with Tukey's multiple comparisons
717 test, *p-value<0.05, *** p-value<0.0005, ns = non-significant.
718 **D)** Whole mount fluorescent immunohistochemistry (GFP and mCherry) of the pancreas of larvae
719 at 14dpt. 3D projection (stack) of *Tg(ins:NTR-P2A-mCherry) ; Tg(nkx6.1:GFP)* one non-ablated
720 and one ablated representative control samples and *Tg(UAS:CaN^{CA}); Tg(ins:NTR-P2A-mCherry)*
721 *; Tg(cftr:gal4)* one non-ablated and one ablated representative samples. The principal islet (PI)
722 and the pancreatic tail are showed. Arrows point out mCherry+ beta cells in the pancreatic tail.
723 Scale 100µM.
724 **E)** Barplot representing the mean number of mCherry+ beta cells in the pancreatic tail of larvae
725 at 14dpt. The gray spheres represent non-ablated *Tg(ins:NTR-P2A-mCherry) ; Tg(nkx6.1:GFP)*
726 condition ; the pink triangles represent the ablated *Tg(ins:NTR-P2A-mCherry) ; Tg(nkx6.1:GFP)*
727 condition ; the black squares non-ablated *Tg(UAS:CaN^{CA}); Tg(ins:NTR-P2A-mCherry) ;*
728 *Tg(cftr:gal4)* condition and inverted green triangles ablated *Tg(UAS:CaN^{CA}); Tg(ins:NTR-P2A-*
729 *mCherry) ; Tg(cftr:gal4)* condition. Data are presented as mean values ± SD. Two-way ANOVA
730 with Tukey's multiple comparison test, *** means p-value<0.0005, **** p-value<0.00005, ns
731 = non-significant.

732 **<u>Figure 4:</u>** *CaN repression potentializes the effect of Notch inhibition on beta cell formation*

733 **A)** Experimental design for Notch inhibition test in non-ablated condition. Larvae were treated
734 concomitantly with LY411575 (Notch inhibitor) and CsA from 3 to 4dpf and were fixed and
735 analyzed at 6dpf.
736 **B)** Graph representing the mean number of mCherry+ beta cells in the pancreatic tail of
737 *Tg(ins:NTR-P2A-mCherry) ; Tg(nkx6.1:GFP)* larvae at 6 dpf depending the concentration of
738 LY411575. The blue dots represent LY411575; and purple combination of LY411575 and CsA.
739 Data are presented as mean values ± SEM. Two-way ANOVA test with Sidak's multiple
740 comparison test, *p-value<0.05, **p-value<0.05, ns = non-significant.
741 **C)** Whole mount fluorescent immunohistochemistry (GFP and mCherry) of the pancreas of
742 *Tg(ins:NTR-P2A-mCherry) ; Tg(nkx6.1:GFP)* larvae at 6dpf. 3D projection (stack) of one control
743 (without any treatment) ; one CsA-treated ; one LY411757-treated and one with both CsA and
744 LY411575 treated larvae. The principal islet (PI) and the pancreatic tail are showed. Arrows
745 point out mCherry+ beta cells in the pancreatic tail. Scale 50µM.
746 **D)** Barplot representing the mean number of mCherry+ beta cells in the pancreatic tail of
747 *Tg(ins:NTR-P2A-mCherry) ; Tg(nkx6.1:GFP)* larvae at 6dpf. The black dots represent the
748 control; gray CsA treatment ;blue LY411575; and purple combination of LY411575 and CsA.
749 Data are presented as mean values ± SD. Two-way ANOVA with Tukey multiple comparison
750 test, ***p-value<0.0005, ****p-value<0.00005.
751 **E)** Graph representing the mean number of mCherry+ beta cells in the pancreatic tail of
752 *Tg(ins:NTR-P2A-mCherry) ; Tg(nkx6.1:GFP)* larvae at 5-6-7 dpf. The black dots represent the
753 control; gray CsA treatment ;blue LY411575; and purple combination of LY411575 and CsA.

754 Data are presented as mean values ± SEM. Two-way ANOVA test with Sidak's multiple
755 comparison test, *p-value<0.05.

756 **Figure 5:** *CaN repression increases the proportion of ductal proliferating cells*

757 **A)** Experimental design for EdU assay in Notch test. Larvae were treated concomitantly with
758 LY411575 (Notch inhibitor) and CsA from 3 to 4dpf and then briefly treated with EdU before
759 fixation and analysis at 4 dpf or at 6dpf.
760 **B)** Whole mount fluorescent immunohistochemistry (GFP and EdU) of the pancreatic tail of
761 *Tg(ins:NTR-P2A-mCherry) ; Tg(nkx6.1:GFP)* larvae at 4dpf. 3D projection (stack) of one control
762 (without any treatment), one with CsA only, one with LY411575 only and one with both CsA
763 and LY411757 representative samples. Scale 50µM.
764 **C)** Barplot representing the percentage of GFP+ ductal cells which incorporated EdU+ in
765 pancreatic tail of *Tg(ins:NTR-P2A-mCherry) ; Tg(nkx6.1:GFP)* larvae for the Notch test. The
766 black dots represent the control; gray CsA treatment ;blue LY411575; and purple combination
767 of LY411575 and CsA. Data are presented as mean values ± SD. T-test. Two-way ANOVA test
768 with Tukey's multiple comparisons test, *p-value<0.05 ; ****p-value<0.00005 ; ns = non-
769 significant.
770 **D)** Barplot representing the number of GFP+ ductal cells which in pancreatic tail of *Tg(ins:NTR-*
771 *P2A-mCherry) ; Tg(nkx6.1:GFP)* larvae at 6dpf for the Notch test. The black dots represent the
772 control; gray CsA treatment ;blue LY411575; and purple combination of LY411575 and CsA.
773 Data are presented as mean values ± SD. T-test. Two-way ANOVA test with Tukey's multiple
774 comparisons test, *p-value<0.05 ; ****p-value<0.00005 ; ns = non-significant.
775 **E)** Experimental design for EdU assay in regeneration. Larvae were treated with nifurpirinol for
776 beta cell ablation from 3 to 4dpf then with CsA from 4 to 5dpf and then briefly treated with
777 EdU before fixation and analysis.
778 **F)** Whole mount fluorescent immunohistochemistry (GFP and EdU) of the pancreatic tail of
779 *Tg(ins:NTR-P2A-mCherry) ; Tg(nkx6.1:GFP)* larvae at 5dpf. 3D projection (stack) of one
780 representative sample of non-ablated or ablated with or without CsA are shown. Scale 50µM.
781 **G)** Barplot representing the percentage of GFP+ ductal cells which incorporated EdU+ in
782 pancreatic tail of *Tg(ins:NTR-P2A-mCherry) ; Tg(nkx6.1:GFP)* larvae at 5dpf. The gray spheres
783 represent non-ablated condition ; the pink triangles the ablated condition ; the black squares
784 CsA condition and inverted green triangles ablated + CsA condition. Data are presented as
785 mean values ± SD. Two-way ANOVA test with Tukey's multiple comparisons test, *p-
786 value<0.05 ; ****p-value<0.00005 ; ns = non-significant.
787 **H)** Whole mount fluorescent immunohistochemistry (VenusPest and EdU) of the pancreatic tail
788 of *Tg(ins:NTR-P2A-mCherry) ; Tg(tp1:VenusPest)* larvae at 5dpf. 3D projection (stack) of one
789 representative sample of non-ablated or ablated with or without CsA are shown. Scale 50µM.
790 **I)** Barplot representing the percentage of GFP+ ductal cells which incorporated EdU+ in
791 pancreatic tail of *Tg(ins:NTR-P2A-mCherry) ; Tg(tp1:VenusPest)* larvae at 5dpf. The gray
792 spheres represent non-ablated condition ; the pink triangles the ablated condition ; the black
793 squares CsA condition and inverted green triangles ablated + CsA condition. Data are
794 presented as mean values ± sd. Two-way ANOVA test with Tukey multiple comparisons test,
795 *p-value<0.05 ; ****p-value<0.00005 ; ns means non-significant.
796 **J)** Barplot representing the number of VenusPest+ ductal cells which incorporated EdU+ in
797 pancreatic tail of *Tg(ins:NTR-P2A-mCherry) ; Tg(tp1:VenusPest)* larvae at 5dpf. The gray
798 spheres represent non-ablated condition ; the pink triangles the ablated condition ; the black
799 squares CsA condition and inverted green triangles ablated + CsA condition. Data are

800 presented as mean values ± SD. Two-way ANOVA test with Tukey's multiple comparisons test,
801 **p-value<0.005.
802

803 **Figure 6:** *CaN regulation is important in juveniles/adults and necessary for correct glycemia recovery*

804 **A)** Whole mount fluorescent immunohistochemistry (GFP and mCherry) of the pancreas of
805 *Tg(ins:NTR-P2A-mCherry) ; Tg(nkx6.1:GFP)* 2 months old zebrafish at 7dpt. 3D projection (stack)
806 of non-ablated and ablated larvae treated with DMSO or CsA representative samples. The
807 principal islet (PI) and the pancreatic tail are shown. Zoom from section of the pancreatic tail
808 are shown, arrows point out mCherry+ beta cells in these zoom. Scale 200µM

809 **B-C)** Barplot representing the number of number of mCherry+ small secondary islets (=<5 cells) in
810 the pancreatic tail of *Tg(ins:NTR-P2A-mCherry) ; Tg(nkx6.1:GFP)* 2 months old zebrafish at 7 **(B)** and
811 10dpt **(C).** The gray spheres represent non-ablated condition ; the pink triangles represent the
812 ablated condition ; the black squares CsA condition and inverted green triangles ablated + CsA
813 condition. Data are presented as mean values ± SD. Two-way ANOVA with Tukey's multiple
814 comparison test, *p-value<0.05.

815

816 **D-E)** Barplot representing the glycemia (mg/dL) of *Tg(ins:NTR-P2A-mCherry) ;* months old adult
817 zebrafish at 7 **(D)** and 10dpt **(E).** The pink triangles represent the ablated condition ; the inverted
818 green triangles ablated + CsA condition; the blue squares *Tg(hsp70:CaN^{CA})* after heat shocks ; the
819 orange lozenges *Tg(UAS:CaN^{CA})*; *Tg(cftr:gal4)*. The grey line represents the mean glycemia of
820 controls (non-ablated) fish. Data are presented as mean values ± SD. One-way ANOVA with Tukey's
821 multiple comparison test, *p-value<0.05; **p-value<0.005.

822

823 **Figure 7:** *Model of CaN action on ductal progenitors to regenerate beta cells*

824 **A)** Under physiological conditions, the behavior of the ductal progenitors is determined by
825 Notch signaling. Calcineurin is active in these progenitors and enable a proper control
826 between proliferation and differentiation. When CaN in repressed, more ductal
827 progenitors enter in the cell cycle (2dpt) and switch to a mode of proliferation leading to
828 differentiation of the two daughter cells (4dpt), as more pro-endocrine cells are formed.
829 The result is a exhaustion of the progenitors and a premature beta cell differentiation
830 (10dpt).

831

832 **Figure 1 supplemental :** *Transcriptomic profiling of ductal cells during beta cell regeneration and*
833 *validation in larvae*

834 A) Design of the experimental pipeline for transcriptomic experiment

835 B) Expression of *ppp3cca; ppp3ccb ; nfatc3a ; nfatc3b* in acinar, alpha, beta, delta or ductal cells
836 population from the zebrafish pancreas [40].

837 C) Calcineurin (*ppp3ccb and ppp3cca)* and NFATc3 (*nfatc3a and nfatc3b)* expression in ductal cells
838 from zebrafish in non-ablated and ablated conditions.

839 **Figure 2 supplemental :** *Calcineurin inhibition with CsA increases the ductal regenerative response*

840 **A)** Whole mount fluorescent immunohistochemistry (mCherry) of the pancreas of *Tg(ins:NTR-*
841 *P2A-mCherry)* larvae at 4-7 and 14dpt. 3D projection (stack) of ablated larvae treated with
842 DMSO or CsA representative samples. The principal islet (PI) and the pancreatic tail are shown.
843 Scale 50 or 100µM.

844 **B-C)** Barplot representing the number of mCherry+ beta cells in the principal islet (PI) **(B)** and the
845 number of secondary islets of mCherry+ beta cells in the pancreatic tail **(C)** of Tg(ins:NTR-P2A-
846 mCherry) ; Tg(nkx6.1:GFP) larvae at 10dpt. Data are presented as mean values ± SD. T-test or
847 Two-way ANOVA with Tukey's multiple comparison test. **p-value<0.005

848 **D)** Barplot representing the number of sst1.1+ mCherry+ bi-hormonal cells in the principal islet
849 (PI) of Tg(ins:NTR-P2A-mCherry) ; Tg(sst1.1:GFP) larvae at 6dpt. Data are presented as mean
850 values ± SD. T-test.

851 **E)** Experimental design for EdU assay in larvae. After NFP treatment for 3 to 4dpf, larvae were
852 exposed to EdU before fixation for analysis.

853 **F)** Whole mount fluorescent immunohistochemistry (GFP and EdU) of the pancreas of
854 Tg(ins:NTR-P2A-mCherry) ; Tg(neurod1:GFP) larvae at 2-4-7 and 10 dpt. 3D projection (stack) of
855 non-ablated and ablated larvae treated with DMSO or CsA representative samples. The principal
856 islet (PI) and the pancreatic tail are shown. Scale 50µM.

857 **G-H)** Barplot representing the number of gcg+ alpha cells **(G)**; the number of GFP+ sst1.1 delta
858 cells **(H);** of Tg(*ins:NTR-P2A-mCherry*) ; Tg(*sst1.1:GFP*) larvae at 10dpt. Gcg was detected by IHC.
859 The gray spheres represent non-ablated condition ; the pink triangles represent the ablated
860 condition ; the black squares CsA condition and inverted green triangles ablated + CsA condition.
861 Data are presented as mean values ± SD. Two-way ANOVA with Tukey's multiple comparison
862 test. **p-value<0.005

863

864 **<u>Figure 4 supplemental :</u>** *CaN repression potentializes the effect of Notch inhibition on beta cell*
865 *formation*

866 **A)** Experimental design for Notch inhibition test in non-ablated condition. Larvae were treated
867 concomitantly with LY411575 (Notch inhibitor) and FK506 from 3 to 4dpf and were fixed and
868 analyzed at 5dpf.
869 **B)** Barplot representing the mean number of mCherry+ beta cells in the pancreatic tail of
870 *Tg(ins:NTR-P2A-mCherry) ; Tg(nkx6.1:GFP)* larvae at 5dpf. The black dots represent the control;
871 gray FK506 treatment ;blue LY411575; and purple combination of LY411575 and FK506. Data
872 are presented as mean values ± SD. Two-way ANOVA with Tukey multiple comparison test,
873 *p-value<0.05,**p-value<0.005, ****p-value<0.00005.
874 **C)** Experimental design for Notch inhibition test in non-ablated condition. Larvae were heat-
875 shocked and then directly treated with LY411575 (Notch inhibitor) from 3 to 4dpf and were
876 fixed and analyzed at 6dpf.
877 **D)** Barplot representing the mean number of mCherry+ beta cells in the pancreatic tail of
878 *Tg(hsp70:CaN^{CA})*; *Tg(ins:NTR-P2A-mCherry) ; Tg(nkx6.1:GFP)* larvae at 5dpf. The black dots
879 represent the control; gray heat-shock ;blue LY411575; and purple combination of LY411575
880 and heat-shock. Data are presented as mean values ± SD. Two-way ANOVA with Tukey multiple
881 comparison test, ****p-value<0.00005.
882 **E)** Barplot representing the mean number of mCherry+ beta cells in the pancreatic tail of
883 *Tg(ins:NTR-P2A-mCherry) ; Tg(nkx6.1:GFP)* larvae at 6dpf after Notch inhibition (LY411575),

884 CaN inhibition (CsA) and NFATc inhibition (CHIR99021). Data are presented as mean values ±
885 SD. Two-way ANOVA with Tukey multiple comparison test, *p-value<0.05,**p-value<0.005,
886 ****p-value<0.00005.
887

888 **Figure 5 supplemental:** *CaN repression increases the proportion of duct proliferating cells*

889 **A)** Z-plan pictures of Tg (nkx6.1:GFP); Tg (ins:NTR*-mCherry) larvae that were treated at 3dpf with
890 both CsA 1µM and LY411575 5µM. At 4dpf, the larvae were exposed to EdU 4mM during 8
891 hours, before analysis at 6 dpf.

892 **B-C)** Barplot representing the number of GFP+ ductal cells which in pancreatic tail of *Tg(ins:NTR-*
893 *P2A-mCherry) ; Tg(nkx6.1:GFP)* larvae at 4dpf for the Notch test. **(B)** Mild Notch inhibition with
894 LY411575 5µM and **(C)** stronger Notch inhibition with LY411575 15µM. The black dots represent
895 the control; gray CsA treatment ;blue LY411575; and purple combination of LY411575 and CsA.
896 Data are presented as mean values ± SD. T-test. Two-way ANOVA test with Tukey's multiple
897 comparisons test, *p-value<0.05 ; ****p-value<0.00005 ; ns = non-significant.

898 **Figure 6 supplemental:** *CaN regulation is important in juveniles/adults and necessary for correct*
899 *glycemia recovery*

900 A) Barplot representing the glycemia (mg/dL) of *Tg(ins:NTR-P2A-mCherry) ;* months old adult
901 zebrafish at 14dpt**.** The pink triangles represent the ablated condition ; the inverted green
902 triangles ablated + CsA condition; the blue squares *Tg(hsp70:CaN^{CA}*) after heat shocks. The grey
903 line represents the mean glycemia of controls (non-ablated) fish. Data are presented as mean
904 values ± SD.
905 B) Barplot representing the glycemia (mg/dL) of *Tg(ins:NTR-P2A-mCherry) ; and Tg(UAS:CaN^{CA}*);
906 *Tg(cftr:gal4)* in non-ablated adult zebrafish. Data are presented as mean values ± SD.

907

908

909

910

911

912

913

914

915

916

Figure 5

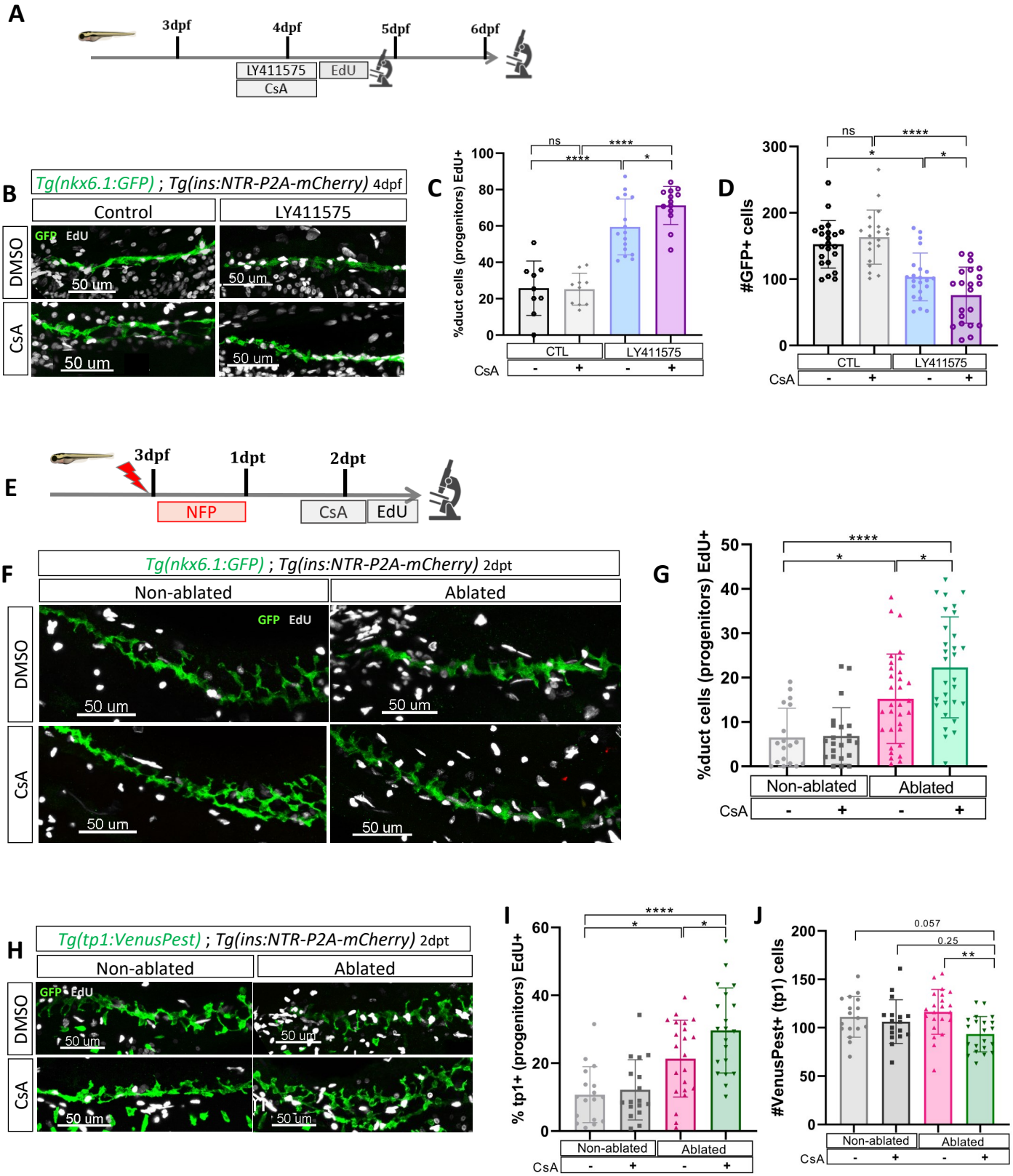
A
3dpf
4dpf
5dpf
6dpf
LY411575
CsA
EdU
B
Tg(nkx6.1:GFP) ; Tg(ins:NTR-P2A-mCherry) 4dpf
Control
LY411575
DMSO
CsA
GFP EdU
50 um
C
%duct cells (progenitors) EdU+
ns
****
*
CTL
LY411575
CsA
D
#GFP+ cells
E
3dpf
1dpt
2dpt
NFP
CsA
EdU
F
Tg(nkx6.1:GFP) ; Tg(ins:NTR-P2A-mCherry) 2dpt
Non-ablated
Ablated
G
%duct cells (progenitors) EdU+
H
Tg(tp1:VenusPest) ; Tg(ins:NTR-P2A-mCherry) 2dpt
I
% tp1+ (progenitors) EdU+
J
#VenusPest+ (tp1) cells
0.057
0.25
**

Figure 4

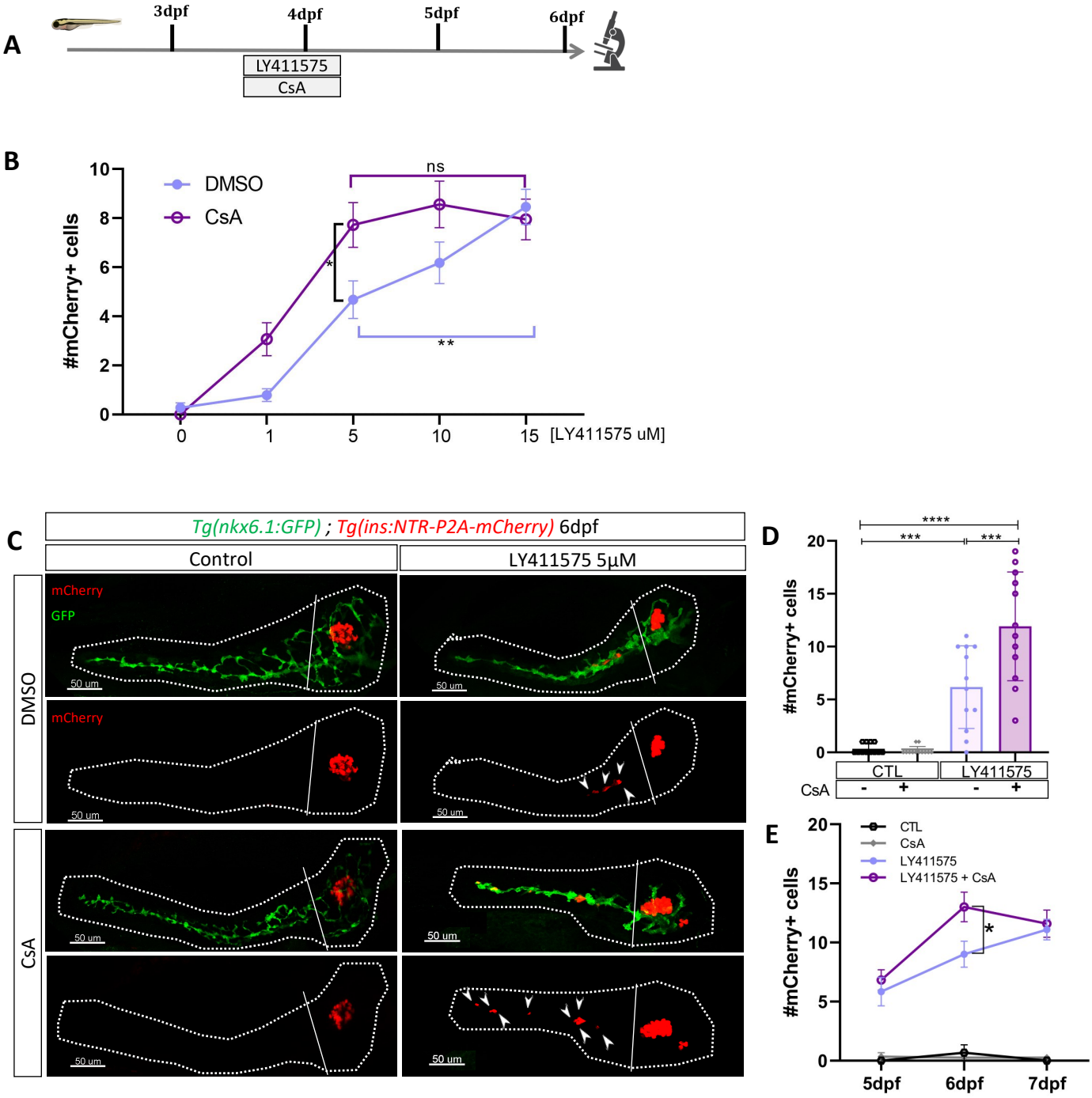
A
3dpf
4dpf
5dpf
6dpf
LY411575
CsA
B
DMSO
CsA
ns
*
**
#mCherry+ cells
[LY411575 uM]
C
Tg(nkx6.1:GFP) ; Tg(ins:NTR-P2A-mCherry) 6dpf
Control
LY411575 5µM
DMSO
CsA
mCherry
GFP
50 um
D
****
***
***
#mCherry+ cells
CTL
LY411575
CsA
E
CTL
CsA
LY411575
LY411575 + CsA
#mCherry+ cells
5dpf
6dpf
7dpf

Figure 1

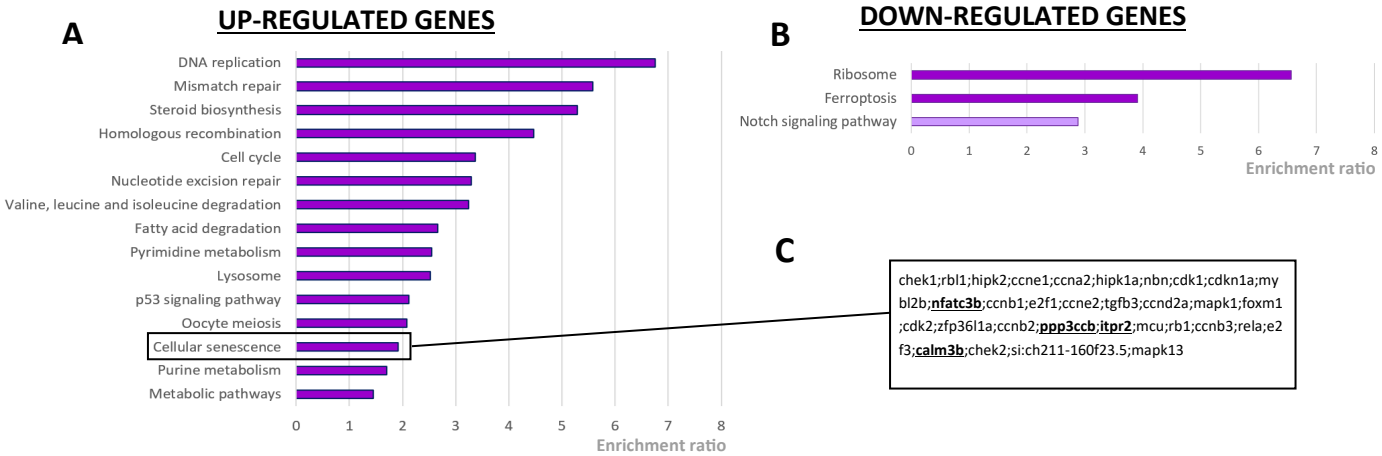
A
UP-REGULATED GENES
DNA replication
Mismatch repair
Steroid biosynthesis
Homologous recombination
Cell cycle
Nucleotide excision repair
Valine, leucine and isoleucine degradation
Fatty acid degradation
Pyrimidine metabolism
Lysosome
p53 signaling pathway
Oocyte meiosis
Cellular senescence
Purine metabolism
Metabolic pathways
0 1 2 3 4 5 6 7 8
Enrichment ratio
B
DOWN-REGULATED GENES
Ribosome
Ferroptosis
Notch signaling pathway
0 1 2 3 4 5 6 7 8
Enrichment ratio
C
chek1;rbl1;hipk2;ccne1;ccna2;hipk1a;nbn;cdk1;cdkn1a;mybl2b;nfatc3b;ccnb1;e2f1;ccne2;tgfb3;ccnd2a;mapk1;foxm1;cdk2;zfp36l1a;ccnb2;ppp3ccb;itpr2;mcu;rb1;ccnb3;rela;e2f3;calm3b;chek2;si:ch211-160f23.5;mapk13

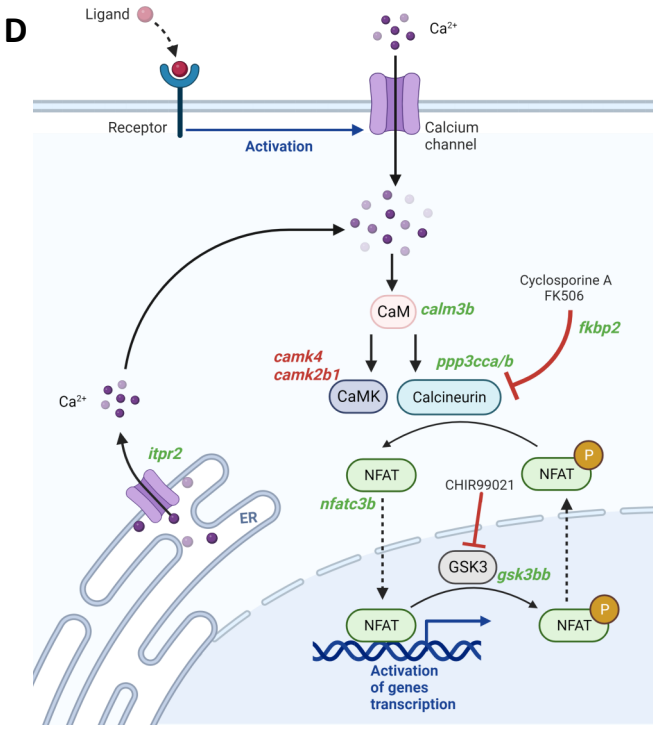
D
Ligand
Ca2+
Receptor
Activation
Calcium channel
Cyclosporine A
FK506
CaM
calm3b
fkbp2
camk4
camk2b1
ppp3cca/b
CaMK
Calcineurin
Ca2+
itpr2
ER
NFAT
P
CHIR99021
nfatc3b
GSK3
gsk3bb
Activation of genes transcription

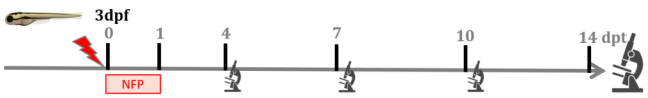
E
3dpf
0
1
4
7
10
14 dpt
NFP

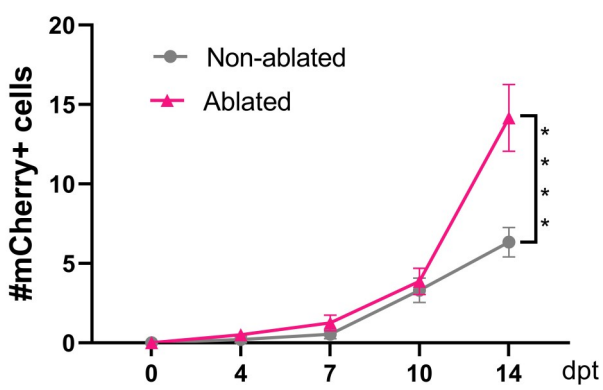
F
#mCherry+ cells
Non-ablated
Ablated
0
5
10
15
20
0
4
7
10
14
dpt
*
*
*
*

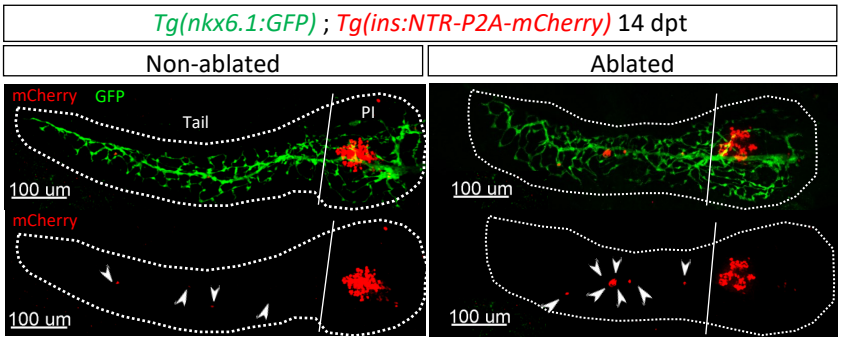
G
Tg(nkx6.1:GFP) ; Tg(ins:NTR-P2A-mCherry) 14 dpt
Non-ablated
Ablated
mCherry GFP
Tail
PI
100 um
mCherry
100 um
100 um
100 um

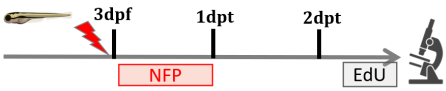
H
3dpf
1dpt
2dpt
NFP
EdU

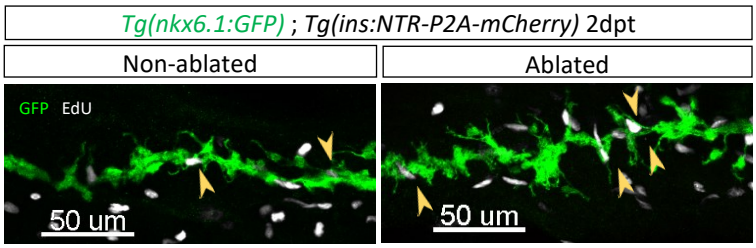
I
Tg(nkx6.1:GFP) ; Tg(ins:NTR-P2A-mCherry) 2dpt
Non-ablated
Ablated
GFP EdU
50 um
50 um

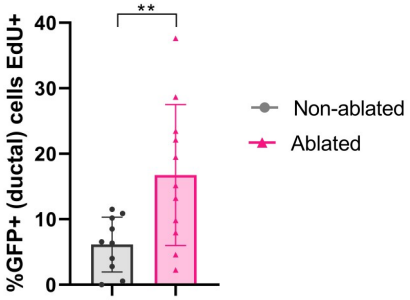
J
%GFP+ (ductal) cells EdU+
0
10
20
30
40
**
Non-ablated
Ablated

Figure 2

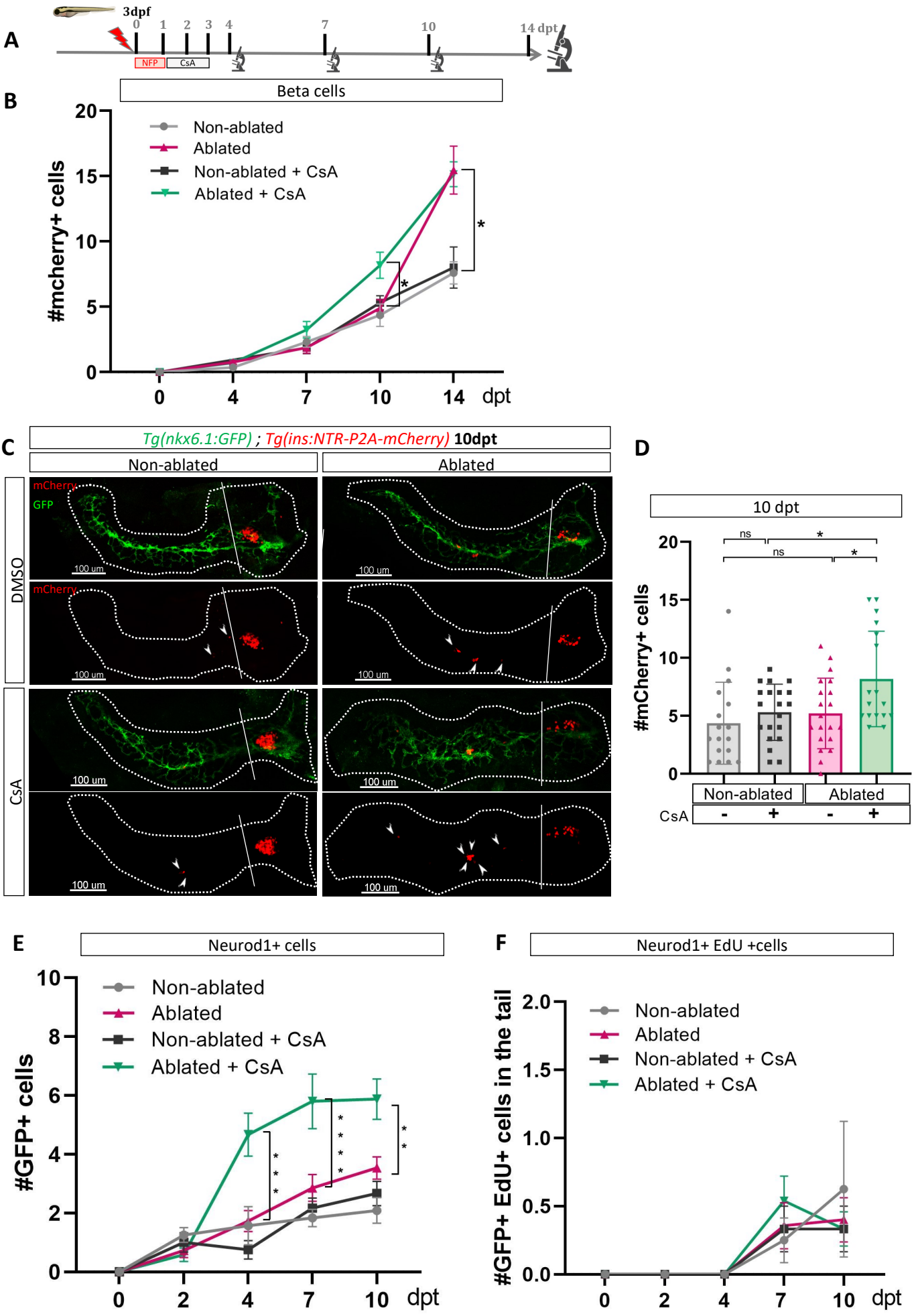
A
3dpf
0
1
2
3
4
7
10
14 dpt
NFP
CsA
B
Beta cells
#mcherry+ cells
Non-ablated
Ablated
Non-ablated + CsA
Ablated + CsA
dpt
C
Tg(nkx6.1:GFP) ; Tg(ins:NTR-P2A-mCherry) 10dpt
Non-ablated
Ablated
DMSO
CsA
mCherry
GFP
100 um
D
10 dpt
#mCherry+ cells
ns
Non-ablated
Ablated
CsA
E
Neurod1+ cells
#GFP+ cells
Non-ablated
Ablated
Non-ablated + CsA
Ablated + CsA
dpt
F
Neurod1+ EdU +cells
#GFP+ EdU+ cells in the tail
Non-ablated
Ablated
Non-ablated + CsA
Ablated + CsA
dpt

Figure 3

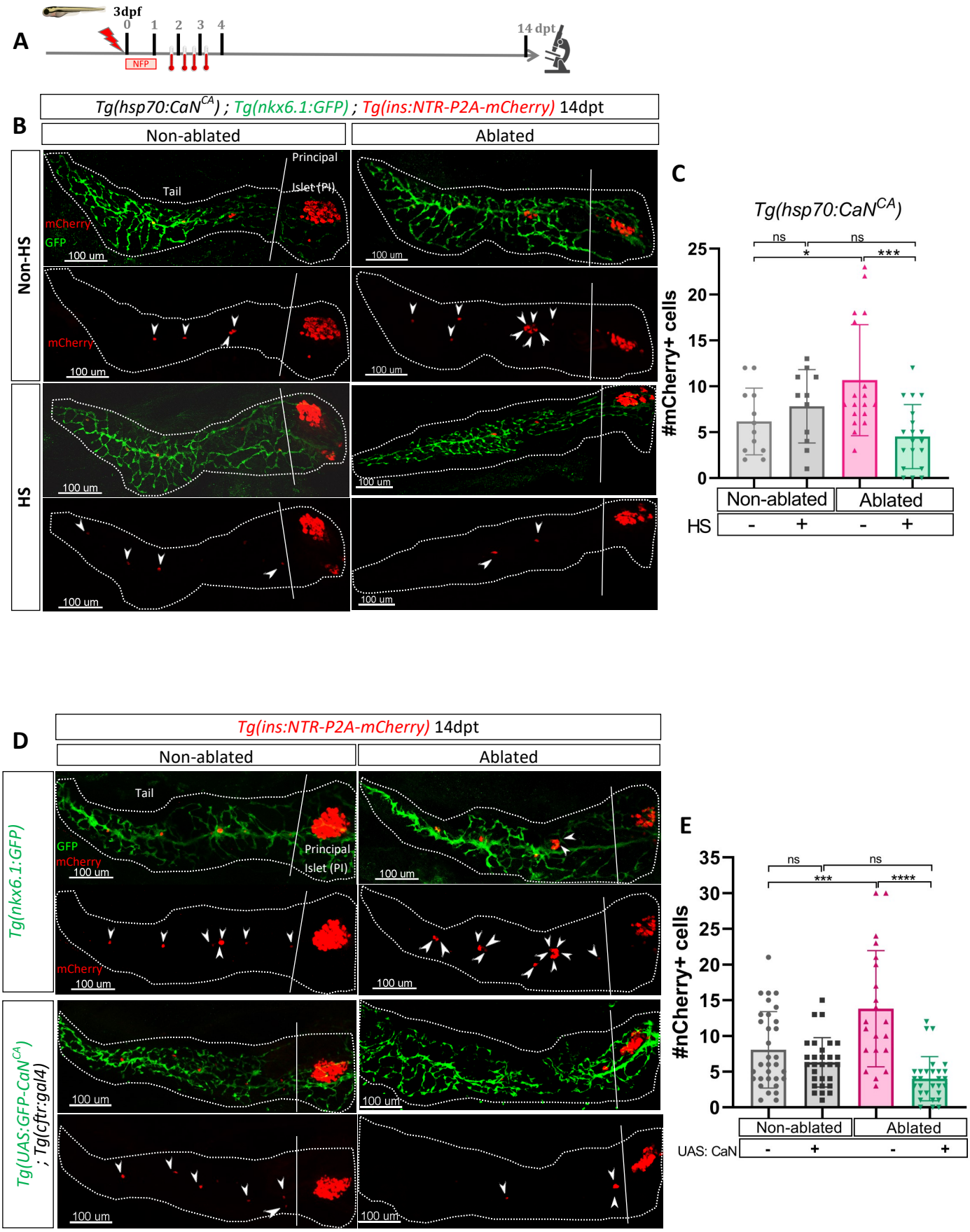
A
3dpf
0 1 2 3 4
NFP
14 dpt
B
Tg(hsp70:CaN^CA) ; Tg(nkx6.1:GFP) ; Tg(ins:NTR-P2A-mCherry) 14dpt
Non-ablated
Ablated
Non-HS
HS
Tail
Principal Islet (PI)
mCherry
GFP
100 um
C
Tg(hsp70:CaN^CA)
#mCherry+ cells
ns
*
***
Non-ablated
Ablated
HS
D
Tg(ins:NTR-P2A-mCherry) 14dpt
Tg(nkx6.1:GFP)
Tg(UAS:GFP-CaN^CA) ; Tg(cftr:gal4)
E
#nCherry+ cells
****
UAS: CaN

Figure 6

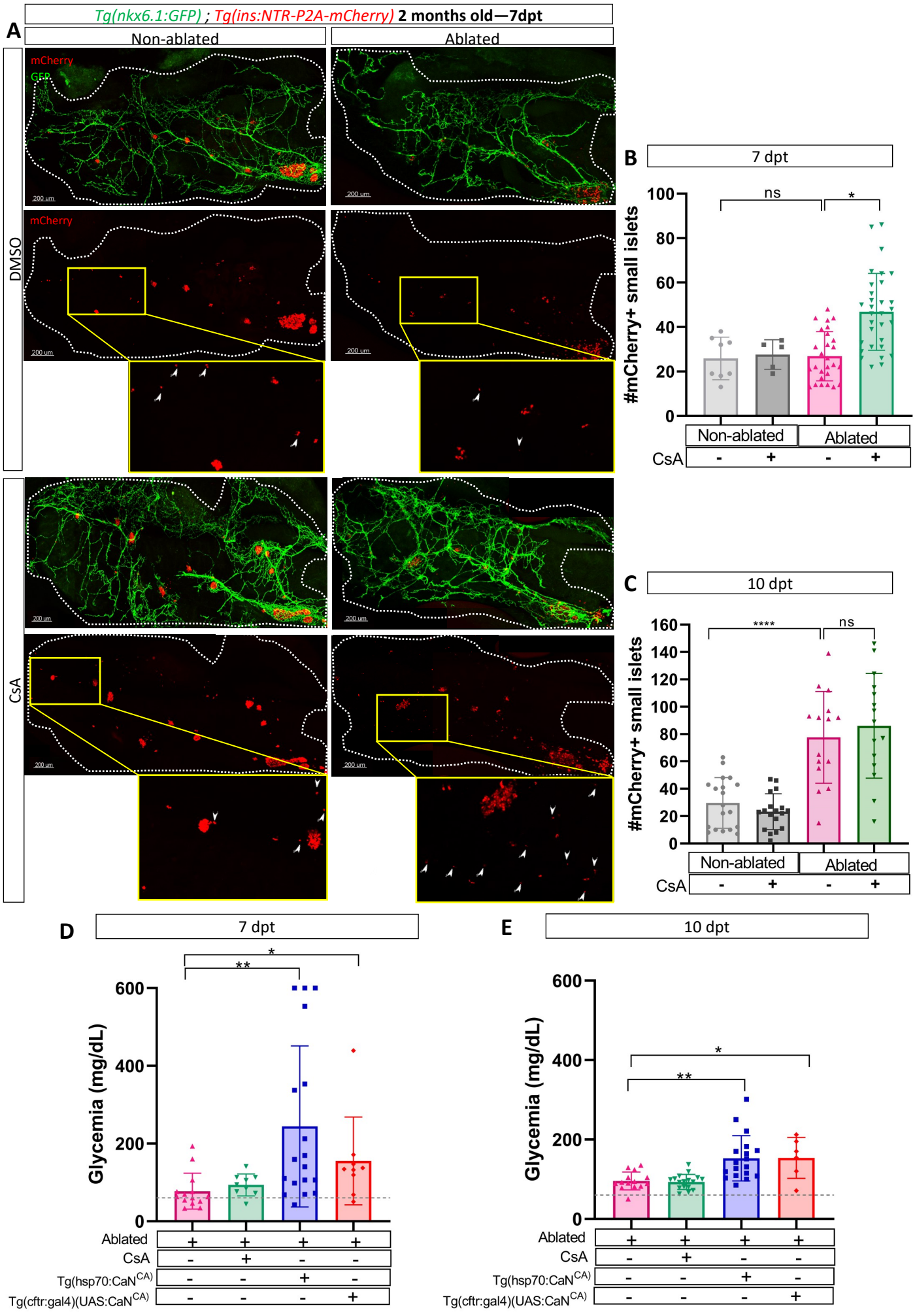
A
Tg(nkx6.1:GFP) ; Tg(ins:NTR-P2A-mCherry) 2 months old—7dpt
Non-ablated
Ablated
mCherry
GFP
DMSO
CsA
200 um
B
7 dpt
#mCherry+ small islets
ns
*
Non-ablated
Ablated
CsA
C
10 dpt
****
ns
D
7 dpt
Glycemia (mg/dL)
Ablated
CsA
Tg(hsp70:CaN^CA)
Tg(cftr:gal4)(UAS:CaN^CA)
E
10 dpt

Figure 7

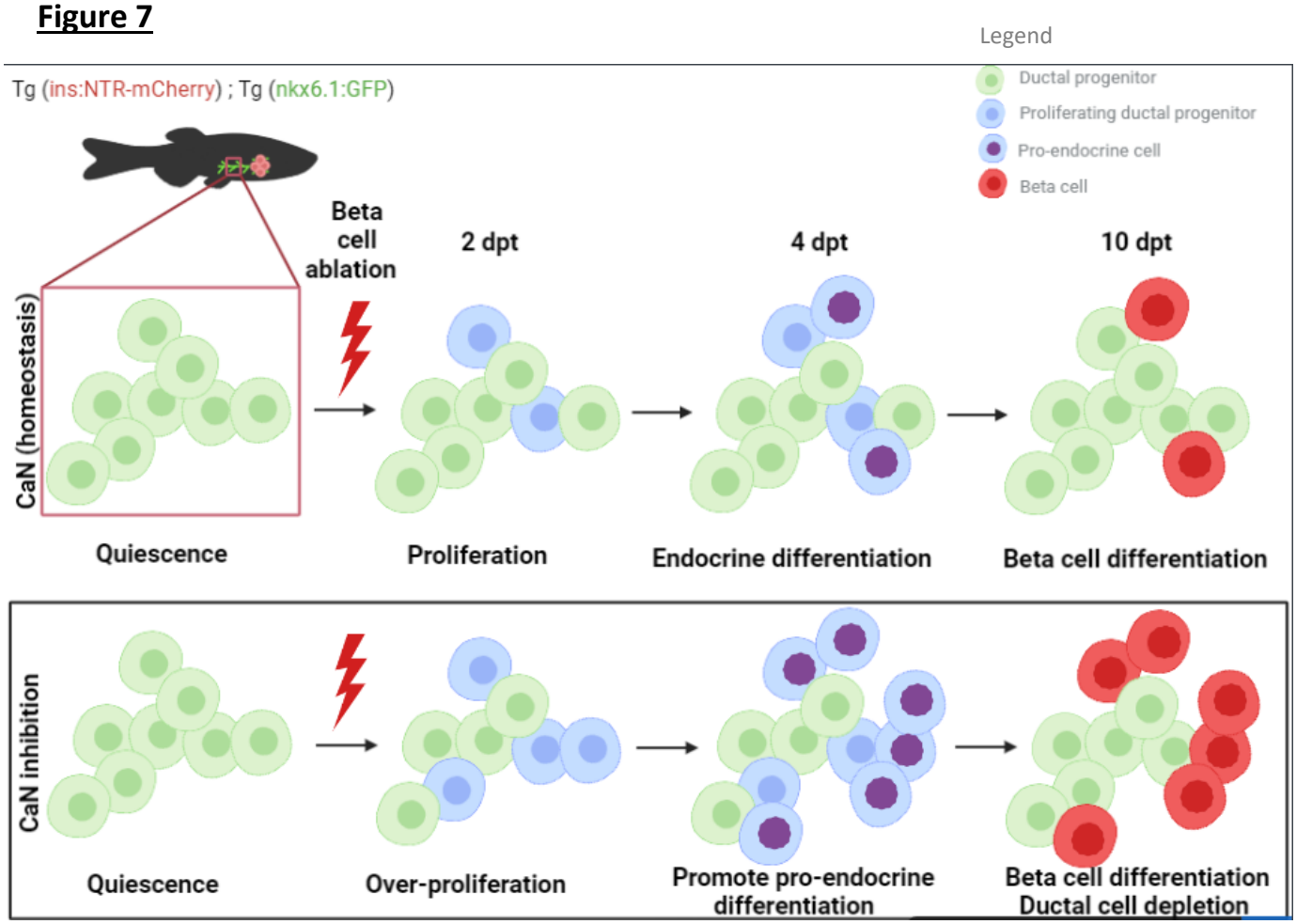
Legend
Ductal progenitor
Proliferating ductal progenitor
Pro-endocrine cell
Beta cell
Tg (ins:NTR-mCherry) ; Tg (nkx6.1:GFP)
Beta cell ablation
2 dpt
4 dpt
10 dpt
CaN (homeostasis)
Quiescence
Proliferation
Endocrine differentiation
Beta cell differentiation
CaN inhibition
Quiescence
Over-proliferation
Promote pro-endocrine differentiation
Beta cell differentiation
Ductal cell depletion